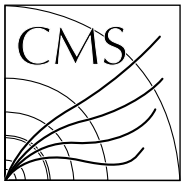

CERN/LHCC 2007-021
LHCC-G-134
29 June 2007

CMS High Level Trigger

CMS Collaboration

Abstract

At the startup of the LHC the CMS DAQ system is expected to be able to sustain an event readout rate of up to 50 kHz from the Level-1 trigger. These events will be read into the Event Filter farm which will run the "High-Level trigger" (HLT) selection algorithms and will accept a rate of up to 300Hz for output to permanent storage. This note documents our current understanding of the physics and computing performance of the HLT algorithms and is a refinement of earlier similar studies. We present a candidate trigger menu for a start-up luminosity of 10^{32} cm^{-2} s^{-1}. A realistic HLT input event variety is obtained by using the Level-1 trigger emulator on the very large QCD backgrounds, a mixture of heavy-quark and vector boson decays to leptons. Applying the standard CMS safety factors used in allocating trigger bandwidth to physics channels, the trigger menu corresponds to a Level-1 trigger accept rate of about 17 kHz and a HLT accept rate of 150 Hz. The average time taken for HLT selection is estimated to be 43 ms for the admixture of events passing the Level-1 trigger.

Chapter 1

Introduction

As documented previously, physics at the LHC begins on-line. At the expected energy and instantaneous luminosities the interaction rate is orders of magnitude larger than what can be reasonably archived for later off-line analysis. The online selection system therefore has to provide a high selectivity of $\sim 10^{-4} - 10^{-5}$ with respect to the active bunch crossings at the LHC.

In the CMS design, this selectivity is achieved in two physical steps, namely the Level-1 Trigger and the High-Level Trigger. The first analyzes each 25-ns crossing within a latency of $3\ \mu$s, whereas the second can operate on longer timescales – but always consistent with the overall Level-1 accept rate. The Level-1 trigger is built of mostly custom-made hardware dedicated to analyzing the detector information in a fairly coarse-grained scale. A key feature of the CMS HLT system is its implementation in a single processor farm (referred to as the "Event Filter Farm"). As a result, in inspecting the events that have passed the Level-1 trigger the full event information is available to a fully programmable processor. The disadvantage of this solution is that the farm must sustain a higher event rate on input – and must also provide more significant CPU resources – than if the HLT had been implemented in multiple physics steps (e.g. a Level-2 and a Level-3 step).

As described in previous CMS Technical Design Reports on the DAQ/HLT and on the Physics Performance of the experiment [1–3], the HLT selection is implemented as a sequence of reconstruction and selection steps of increasing complexity, reconstruction refinement and physics sophistication. The fully programmable nature of the processors in the Event Filter Farm enables the implementation of very complex algorithms utilizing any and all information in the event.

The current study represents a substantial refinement with respect to those previously submitted to the LHCC for the following reasons:

- All HLT algorithms have been implemented using the latest CMS software, the `CMSSW` suite which is expected to be the software CMS will actually take and analyze data with. The release used in these studies was `CMSSW_1_3_1_HLT6`, a branch created for dedicated trigger development and studies.
- The events used for HLT studies are passed through a Level-1 trigger emulator which essentially duplicates the behavior of the Level-1 trigger hardware at the bit level.
- A complete trigger table is built and its performance as a whole (e.g. including overlaps across triggers) is evaluated.
- An extended effort on optimizing the CPU performance of the HLT selection has

yielded very encouraging results presented in this note.

The entire study was designed to be as realistic as possible. It concentrated on conditions close to the startup of the LHC, and thus all studies have assumed an instantaneous luminosity of 10^{32} cm^{-2} s^{-1}. Moreover, the CPU time measurements were all performed on a Core 2 5160 Xeon processor running at 3.0 GHz, i.e. using a processor that is very close to the one that is likely to be procured for the Event Filter Farm prior to data-taking in 2008.

In the following chapters we review the Level-1 and HLT algorithms that result in the physics objects selected by the Event Filter Farm. We subsequently describe "cross-triggers" i.e. triggers requiring different objects (e.g. an electron and a muon). The performance of a combined trigger table is discussed next. We conclude with a brief description of possible improvements in the ongoing work to optimize the physics and CPU performance of the HLT selection.

Chapter 2

Triggers for muons

Muons will be used to calibrate detectors, perform precision studies of the Standard Model and search for new physics. Many interesting physics signals contain leptons isolated from any hadronic activity, whereas the dominant component of the muon trigger rate consists of leptons from hadron decays. This is exploited at the trigger level by applying isolation criteria and lowering the p_T thresholds, thus optimizing the physics reach of the experiment.

This chapter presents the HLT reconstruction strategy for muons and the performance of the main muon triggers: single and double-muon with and without isolation criteria. Additional muon triggers, mostly intended for calibration purposes or for specific physics signatures are also included in the trigger table.

2.1 Level-1 Trigger

The Level-1 muon trigger provides a fast estimate of the transverse momentum (p_T) of muons via look-up tables. Three different trigger subsystems contribute to this purpose: the Drift Tube (DT) and Cathode Strip Chamber (CSC) subsystems, which cover the rapidity regions $|\eta| < 1.2$ and $0.9 < |\eta| < 2.4$, respectively, and the Resistive Plate Chamber (RPC) subsystem which operates in the range $|\eta| < 2.1$ ($|\eta| < 1.6$ for the CMS start-up phase). The overlap between these subsystems ensures high efficiency and redundancy over most of the muon spectrometer coverage. The DT and CSC subtriggers determine the muon p_T from the difference between segment slopes in successive layers of the muon spectrometer, whereas the RPC subtrigger compares the observed muon trajectory with predefined hit patterns as a function of p_T. All sub-triggers assume that muons are produced in a region around the LHC beam spot. More details on the Level-1 muon trigger components and logic can be found in [1, 4].

The Global Muon Trigger system is responsible for matching DT and CSC candidates with RPC candidates, as well as for rejecting unconfirmed candidates of low quality. Up to four muon candidates satisfying some minimal quality criteria and with the highest p_T are forwarded to the HLT for further processing. The two main Level-1 muon sub-triggers are the single-muon and double-muon triggers.

The type of events contribute to the Level-1 muon trigger rate depends on the p_T threshold used. Pion and kaon decays dominate in the region $p_T \lesssim 5$ GeV. Leptons from b and c-quark decays dominate in the 5 GeV $< p_T <$ 35 GeV range, whereas at higher p_T values, $W \to \mu\nu$ events are the main component of the muons passing the Level-1 criteria. The contribution of decays in flight must be included in rate estimates at higher p_T thresholds due to their very high rate and possible misreconstruction to higher p_T.

At a luminosity of 10^{32} cm^{-2} s^{-1}, the Level-1 single-muon rate is about 1 kHz for thresholds as low as 7 GeV while the di-muon rate is smaller than 200 Hz at the lowest useful threshold of 3 GeV. More detailed information on Level-1 rates as a function of p_T can be found in the Appendix of Ref. [5].

The efficiency times acceptance of the Level-1 single-muon criteria on a $W \rightarrow \mu\nu$ sample generated in the fiducial volume $|\eta| < 2.4$ with $p_T > 10$ GeV is 83%. The combined efficiency of single and double-muon criteria on a $Z \rightarrow \mu\mu$ sample in a similar fiducial volume is 99%.

2.2 HLT algorithms

In the first step of the HLT muon selection, referred to as "Level-2 reconstruction", Level-1 muon candidates are used to seed the reconstruction of tracks in the muon chambers. Level-2 muons are required to exceed p_T threshold values that depend on the trigger path. After efficient reduction of the Level-2 accept rate, the Level-3 reconstruction is carried out by combining Level-2 muons and charged-particle tracks reconstructed in the central tracker. The final filtering step is applied on the precisely measured Level-3 muons.

Isolation is an optional step in HLT reconstruction: only muon paths with isolation criteria require it. Due to the limited CPU resources the isolation requirements are applied as soon as more detailed information on a muon becomes available: calorimeter-based isolation (Level-2) is applied first after Level-2 reconstruction and is then followed by track-based isolation (Level-3), with isolation being applied to pixel and/or regionally-reconstructed tracks. The event can be rejected if there are too few isolated muons, according to the criteria of each trigger path.

The different reconstruction steps are briefly detailed in the following subsections. More details on the HLT reconstruction methods and performance can be found in References [1, 2].

The Level-2 reconstruction, whicih is based on Kalman-filter techniques, starts with an estimation of the seed state using the Level-1 information. In order to optimize the processing time and to avoid possible biases from the Level-1 seed, an initial pattern recognition is carried out to fetch muon segments along the trajectory. A second, more precise fit using all hits in these segments is then performed to determine the muon parameters.

At each step of the Level-2 algorithm the track parameters are propagated to the adjacent layer of muon detectors. A suitable propagator must precisely take into account material effects like multiple scattering and energy losses due to ionization and bremsstrahlung in the muon chambers and in the return yoke. In order to reduce the HLT processing time, a fast Level-2 propagator is used. The trajectory is extrapolated in sequential steps using helix parametrizations. The required precision is obtained by using smaller steps in regions with larger magnetic field inhomogeneities. Multiple scattering and energy losses in each step are estimated from fast parametrizations, avoiding time-consuming accesses to the detailed material and geometry descriptions.

Muons passing the Level-2 selection are input to the Level-3 reconstruction step. The track parameters and uncertainties of the Level-2 muon constrained to the interaction region define a rectangular $\eta\phi$ region in the silicon tracker. Pairs or triplets of hits in the innermost layers of the tracker form trajectory seeds that are required to be compatible with the $\eta\phi$ region and with primary vertex constraints. Trajectories from these seeds are subsequently

grown using Kalman filtering techniques. The best reconstructed trajectory, as determined from a chi-squared test, is chosen. This trajectory is then optionally combined with the reconstructed hits from the original Level-2 muon.

Isolation variables are defined as sums of transverse energies, E_T, in the calorimeter towers (for Level-2) or of transverse momenta, p_T, of charged-particle tracks (for Level-3) found in a cone around the direction of the muon[1] In both cases deposits associated with the candidate muon as well as from other muons in the event are excluded from the sum. The thresholds and cone sizes used are adjusted in different pseudo-rapidity ranges [6] in order to provide an optimal selection of signal vs rejection of backgrounds.

In the Level-2 isolation variable the calorimetry deposits are calculated as a weighted sum of the energies deposited in the ECAL (weight of 1.5) and in the HCAL (weight of 1.0). The unpacking of the ECAL data is done within margins surrounding the L1 seeds. This regional ECAL unpacking approach is approximately a factor of four faster than the full subdetector unpacking, without loss of signal efficiency. The higher ECAL weight reflects the higher sensitivity of the ECAL to low-energy deposits as well as its higher efficiency in detecting neutral particles contained in jets.

In the Level-3 isolation variable only charged-particle tracks near the vertex of the candidate muon are selected. This suppresses contributions from other pp collisions, thus making the Level-3 isolation requirement less dependent on instntaneous luminosity than the corresponding Level-2 isolation.

2.2.1 Special MC samples for muon HLT paths

A large fraction of the Level-1 muon trigger rate is due to low-p_T muons which are reconstructed above the nominal p_T threshold. Most of these muons come from pion and kaon decays. Although the probability of decays in the volume in front of the calorimeter is small, the number of hadrons is very high and therefore this process dominates the Level-1 rate in the low-p_T muon region.

In order to get an enriched sample of muons in this region, pion and kaon decays into muons are forced and an event weight is assigned according to the prescription described in [7]. Significant statistics over the full momentum range are obtained by generating samples of minimum bias events forced to contain a muon in three different p_T intervals: a) $p_T < 4$, b) $p_T > 4$ and c) $p_T > 10$GeV/c (the latter also with a cut of $\hat{p}_T > 10$ on the hard process). The performance of the muon HLT code on the muon-enriched sample was compared with that on minimum bias samples. The trigger rates and average processing times estimated for the various muon HLT paths show good agreement among the two Monte-Carlo samples.

2.3 HLT performance

2.3.1 Trigger rates

Single and double-muon paths, with and without isolation requirements, select a large fraction of the muon events of physics interest. All HLT single-muon paths are seeded by Level-1 candidates passing single-muon criteria ($p_T > 7$ GeV). Similarly, only candidates passing the Level-1 double-muon criteria ($p_T > 3$ GeV) are considered in HLT double-muon paths.

[1]The size of the cone is defined in $\eta - \phi$ space as $R = \sqrt{\Delta\eta^2 + \Delta\phi^2}$ around the direction of the muon at the collision point.

Paths without isolation criteria, which will be denoted as "relaxed paths", are essential to maintain high efficiency for events with high p_T muons, for which the application of isolation criteria is not necessary. The resulting p_T threshold for the relaxed single-muon trigger is 16 GeV, giving a HLT rate of $\lesssim$ 20 Hz, as shown in Figure 2.1. For the relaxed double-muon trigger, the minimal threshold of $p_T > 3$ GeV for both muons guarantees a trigger rate below 20 Hz (Figure 2.2). These low thresholds also allow detailed studies of the performance of HLT isolation algorithms on reference samples like $W \to \mu\nu$ and $Z \to \mu\mu$. Understanding this performance with the W and Z samples will be essential in designing selections for higher LHC luminosities. A breakdown of the different contributions to the HLT rates for these relaxed paths can be found in the Appendix of Ref. [5].

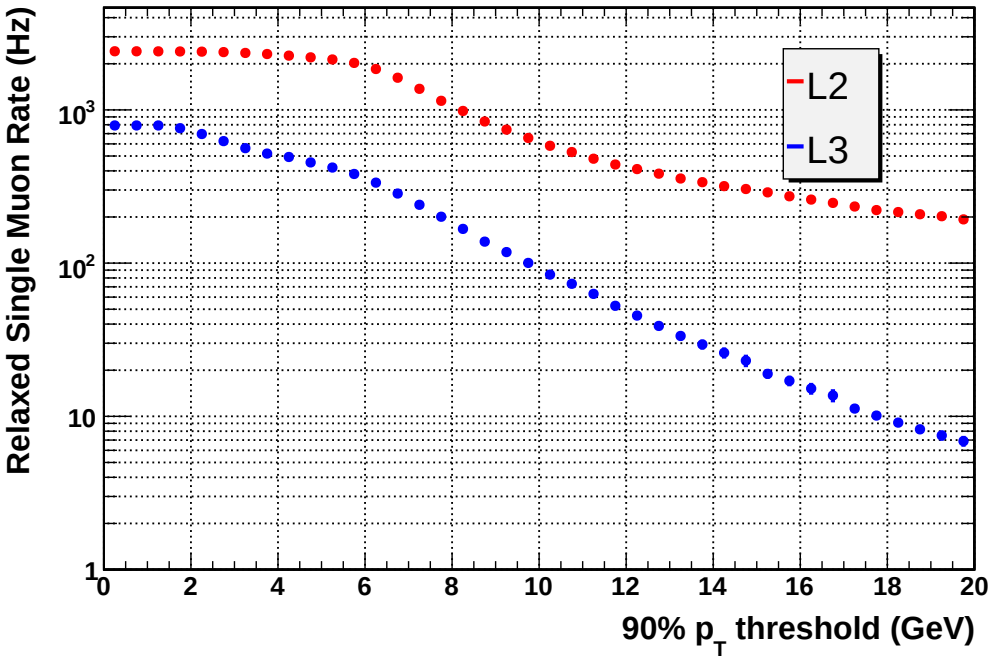

Figure 2.1: HLT rates for the relaxed single-muon path – from the muon-enriched Monte Carlo sample. The rate for a p_T threshold of 16 GeV is $\lesssim$ 20 Hz.

Isolation cuts allow to lower the p_T thresholds for physics analyses requiring isolated muons in the final state. As shown in Figure 2.3 a single isolated muon path with a threshold of $p_T > 11$ GeV can be sustained.

2.3.2 Efficiency

The efficiency of the three trigger paths described above on $W \to \mu\nu$ and $Z \to \mu\mu$ events is shown in Table 2.1.

2.3.3 CPU performance

Table 2.2 shows a summary of the timing for each step of the isolated single-muon path.

2.4 Prescaled muon triggers

The main, unprescaled relaxed single-muon path uses a threshold of $p_T > 16$ GeV, leading to a HLT accept rate of $\lesssim$ 20 Hz. The lowest p_T threshold for a detectable muon in the muon

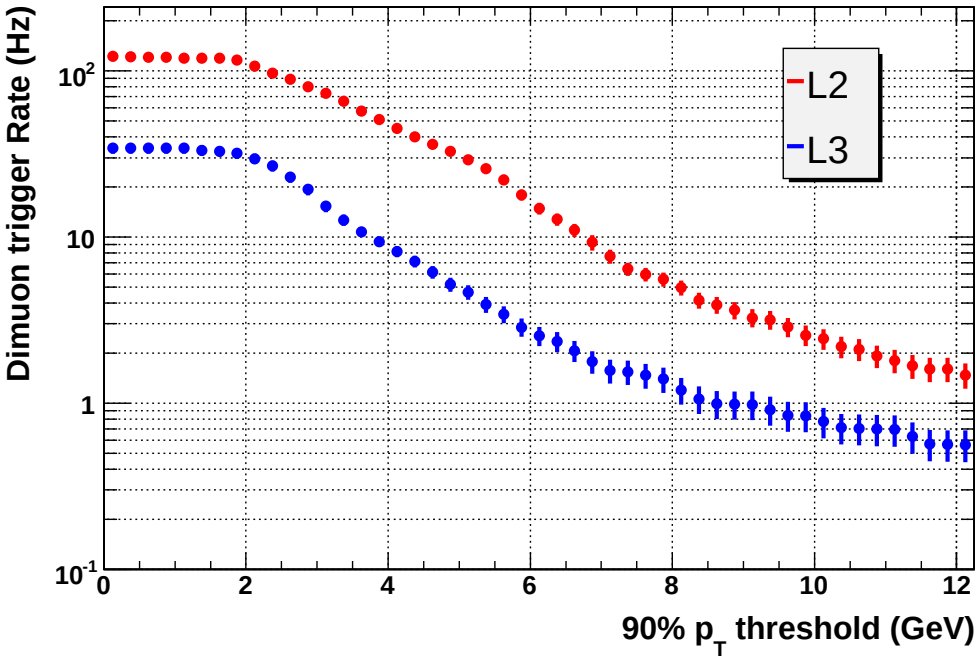

Figure 2.2: HLT rates for the relaxed double-muon path as a function of p_T. QCD, Drell-Yan and additional prompt-J/Ψ contributions not included in standard QCD production have been taken into account. For $p_T > 3$ GeV a HLT rate of ~ 15 Hz is obtained.

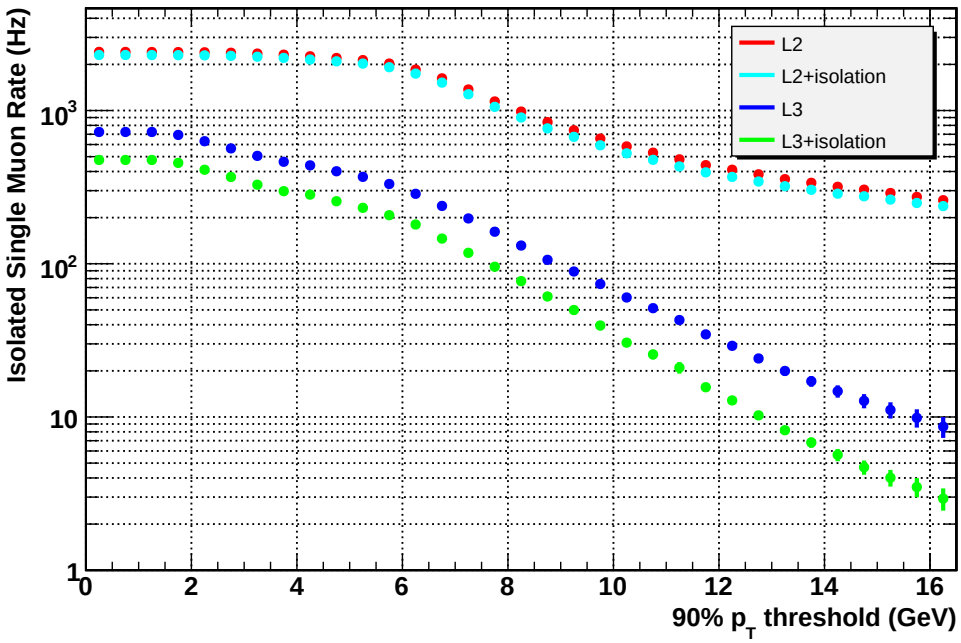

Figure 2.3: HLT rates for the isolated single-muon path on the muon enriched sample. For $p_T > 11$ GeV a HLT rate of ~ 20 Hz is expected.

Signal	HLT Single Relaxed muon eff.(%)	HLT Double muon eff.(%)	HLT Single Isolated muon eff.(%)	(Level-1)*HLT acceptance (%)
$Z \to \mu\mu$	98.6	91.2	95.8	98.1
$W \to \mu\nu$	86.9	-	81.4	76.7

Table 2.1: HLT efficiencies and overall acceptance of muon trigger paths on the benchmark processes $Z \to \mu\mu$ and $W \to \mu\nu$. HLT efficiencies are determined on the total number of events passing the corresponding Level-1 criteria (single or dimuon Level-1 triggers, depending on the case). The overall (Level-1)*HLT acceptance is calculated on the total number of generated events. Both samples have been generated with the following cuts for the muons in the final state: $|\eta| < 2.4$ and $p_T > 10\,\text{GeV}$.

HLT step	Running time (ms)	Averaged time (ms)	Fraction of all L1 events processed
MUON unpacking	3.0	3.0	0.1090
MUON hits and segments	7.0	7.0	0.1090
Level-2 reconstruction	13.8	13.8	0.1090
ECAL unpacking	3.6	0.4	0.0135
HCAL unpacking	0.6	0.1	0.0135
ECAL RecHits	1.7	0.2	0.0135
HCAL RecHits	0.5	0.1	0.0135
CaloTowers	2.6	0.3	0.0135
Level-2 isolation	0.2	0.0	0.0135
Pixel unpacking	1.3	0.1	0.0101
SiStrip unpacking	0.2	0.0	0.0101
Pixel RecHit and clustering	5.5	0.5	0.0101
SiStrip clustering	0.1	0.0	0.0101
Level-3 reconstruction	50.1	4.6	0.0101
Pixel Tracks	6.3	0.1	0.0012
Level-3 isolation	0.1	0.0	0.0012
Total		30.2	

Table 2.2: Running and average processing times for different steps of the isolated single-muon HLT path for Level-1 accepted minimum bias events.

chambers is ~ 3 GeV. We subdivide the available muon low-p_T range, from 3 to 16 GeV, in four intervals. We define Level-1 and HLT paths and prescales to collect data in these four low-p_T regions. The choice of the number of paths, thresholds and prescale values is not unique. The choice discussed here, based on the expected single-muon Level-1 and HLT rates is motivated by the need to collect, in a relatively short period, high statistics data samples for trigger, detector and physics studies. It is expected that such choices will be optimized in the future.

The relaxed single-muon trigger paths, including their Level-1 and HLT p_T thresholds and the proposed prescale values, are shown in Table 2.3. The total HLT output rate of the relaxed single-muon prescaled triggers, with the given prescales, adds up to ~ 3 Hz.

The lowest p_T threshold paths ($p_T > 3$ GeV and $p_T > 5$ GeV) are prescaled at Level-1. The two higher p_T relaxed muon paths, needed to cover the kinematic range between the Level-1 (7 GeV) and the HLT (16 GeV) relaxed muon trigger thresholds, are seeded by the unprescaled single muon L1 (`A_SingleMu7`) bit. This bit is also used to seed the unprescaled

HLT relaxed and tight muon paths. Thus, in this configuration, the HLT prescales do not imply an inefficient use of L1 bandwidth.

The choice of the p_T thresholds for these prescaled triggers is guided by the expected HLT relaxed single-muon rate and the need to have relaxed single-muon data samples, with sufficient statistics over the whole range between 3 and 16 GeV, not covered by the main, unprescaled, relaxed single-muon trigger. The trigger efficiency for each trigger path (but the lowest-p_T one) can be measured using the data sample collected with the neighboring prescaled trigger with a lower p_T threshold.

Table 2.3: The "relaxed single-muon" trigger table, showing the trigger thresholds in p_T, prescale values, expected rates for each trigger path, and the resulting total rate at the HLT level. The reported uncertainties on the rates are from the statistics of the simulated events. The Rel1MuLow3 and Rel1MuLow4 paths are both seeded by the same Level-1 $p_T > 7$ GeV path.

Path Name	Level-1				HLT		
	pT Thresh. (GeV)	Rate (kHz)	Prescale value P1	Presc. Rate (Hz)	pT Thresh. (GeV)	Prescale value P3	Presc. Rate (Hz)
Rel1MuLow4	7	0.78 ± 0.03	1	780 ± 30	10	100	0.75 ± 0.05
Rel1MuLow3	7	0.78 ± 0.03	1	780 ± 30	7	400	0.75 ± 0.02
Rel1MuLow2	5	1.52 ± 0.04	2000	0.76 ± 0.04	5	1	0.7 ± 0.3
Rel1MuLow1	3	3.57 ± 0.07	4000	0.90 ± 0.04	3	1	0.8 ± 0.4
Rel1MuAll							3.0 ± 0.6

Chapter 3

Triggers for electrons and photons

Maintaining a high trigger efficiency for high-transverse momentum electrons and photons is one of the key requirements of the Level-1 and High-Level Trigger systems. Electrons and photons are involved in essentially all scenarios for potential new physics signatures, while they also constitute basic elements of most physics measurements within the Standard Model. We have developed triggers for isolated electrons and photons. In order to study the isolation criteria better we have also included triggers for relaxed electrons and photons. We have also developed a very high energy electron trigger with very loose isolation criteria.

3.1 Level-1 Trigger

The Level-1 trigger algorithm and its implementation has not evolved since the submission of the Trigger and DAQ Tehnical Design Reports [1, 4]. The Level-1 electromagnetic trigger is based on ECAL trigger towers and no attempt is made to distinguish between electrons and photons at this stage. Energy deposits in trigger towers (corresponding to 5×5 crystals in the barrel ECAL and more complicated collections in the endcap ECAL) are classified as isolated or non-isolated according to the requirements described in [1]. The Level-1 trigger is split into four paths, which are listed in Table 3.1 along with the corresponding E_T thresholds. The relaxed triggers accept both isolated and non-isolated trigger deposits and are therefore required to satisfy higher E_T thresholds.

More details on the Level-1 electron/photon trigger components and logic can be found in [1, 4].

Level-1 EM trigger path	E_T threshold (GeV)
Single isolated	12
Single relaxed	15
Double isolated	8
Double relaxed	10

Table 3.1: E_T thresholds for Level-1 EM trigger paths.

The efficiencies of the Level-1 EM trigger paths for signal processes are shown in Table 3.2.

3.2 HLT selection of electrons and photons

The HLT selection for electrons and photons is described in detail in [8]. The selection is performed by applying a sequence of filters of increasing complexity and sophistication,

Signal process	Preselection	Single	Relaxed Single	Double	Relaxed Double	Total L1
$Z \to ee$	45.8	96.0	97.0	77.3	86.9	98.1
$W \to e\nu$	63.1	83.3	85.6	6.2	7.0	89.6
$H \to \gamma\gamma$ (m_H=120 GeV)	71.7	97.9	100.0	77.4	96.0	100.0

Table 3.2: Efficiency of the generator level preselection including detector acceptance (%) and Level-1 trigger efficiencies relative to the preselection (%) for EM trigger paths.

and therefore of increasing CPU requirements as well. Each sequence takes as input the candidates passing the previous filtering step:

HLT trigger path	E_T threshold (GeV)
Single isolated electron	15
Single relaxed electron	17
Double isolated electron	10
Double relaxed electron	12
Single isolated photon	30
Single relaxed photon	40
Double isolated photon	20
Double relaxed photon	20
Single high energy EM	80
Single very high energy EM	200

Table 3.3: E_T thresholds for HLT EM trigger paths.

1. Reconstruction of clusters in the ECAL within regions corresponding to Level 1 triggers in the event. A margin is included around the trigger regions to ensure complete collection of energy. Super-clusters (groups of clusters along a road in the ϕ direction) are constructed to collect bremsstrahlung radiated from electrons or converted photons. The super-cluster transverse energy, E_T, is required to exceed a threshold, with a value dependent on the HLT path – as listed in Table 3.3.

2. ECAL isolation is required (photon and high energy trigger paths only)

3. Reconstruction of energy in the HCAL followed by the requirement of HCAL isolation.

4. Global reconstruction of hits in the pixel detector (electron trigger paths only). The energy and position of the super-cluster are used to propagate back through the magnetic field to search for compatible hits in the first or second layers of the pixel detector within a search area restricted to 40 mrad in ϕ. It is required that an additional hit is found in the second or third pixel layer which satisfies tight requirements on compatibility with the position of the first pixel hit and the position and energy of the super-cluster.

5. Reconstruction of the electron track using the Kalman Filter formalism, starting from a seed formed from the two pixel hits. This is followed by the application of a cut on the ratio of the super-cluster energy to the track momentum (single electron path only).

6. Regional track reconstruction: tracks are seeded from pairs of hits in the pixel layers located within a rectangular $\eta\phi$ region around the direction of the reconstructed electron or photon. The seed positions are also required to be compatible in z with the nominal

vertex spread (photon trigger paths), or with the closest approach of the electron track to the beam line (electron paths).

7. Tracker isolation: For electrons, a threshold is applied on the p_T sum of tracks within a cone around the electron direction, but outside a smaller veto cone in order to exclude the electron track itself. For photons, a threshold is applied on the number of tracks within a cone around the photon direction.

Additional trigger paths are defined for high energy electrons and photons. The input for these paths is the set of events passing the Level-1 relaxed single trigger. The paths are designed to have very high efficiencies in a region with very little background. This is achieved by removing the requirement of a reconstructed track for electrons and relaxing isolation requirements. Two paths are defined: one consisting solely of a requirement that the supercluster E_T exceeds 200 GeV, and a second consisting of a lower E_T threshold (80 GeV) plus the following sequence of filters:

1. ECAL isolation is required.
2. HCAL/ECAL energy ratio is required to be less than 5%.
3. HCAL isolation is required excluding a veto cone to allow for shower leakage into the HCAL.
4. Tracker isolation: the number of tracks within a cone around the electron or photon candidate is required not to exceed 3.

3.3 HLT performance

3.3.1 Trigger Rates

The electron and photon HLT rates versus the E_T threshold applied is shown in Figures 3.1 and 3.2 respectively.

3.3.2 Efficiency

Efficiencies of the egamma HLT paths for signal processes, relative to the set of events passing the corresponding Level-1 trigger, are shown for electrons and for photons in Tables 3.4 and 3.5, respectively. The efficiencies of the high energy paths are given in table 3.6.

Signal process	Isolated single electron	Relaxed single electron	Isolated double electron	Relaxed double electron
HLT: $Z \to ee$	83.3	85.2	63.8	64.4
HLT: $W \to e\nu$	62.5	61.2	-	-
L1*HLT: $Z \to ee$	80.0	82.6	62.6	63.2
L1*HLT: $W \to e\nu$	52.1	52.4	-	-

Table 3.4: Signal efficiencies in % for electron HLT paths with and without folding in L1 efficiency.

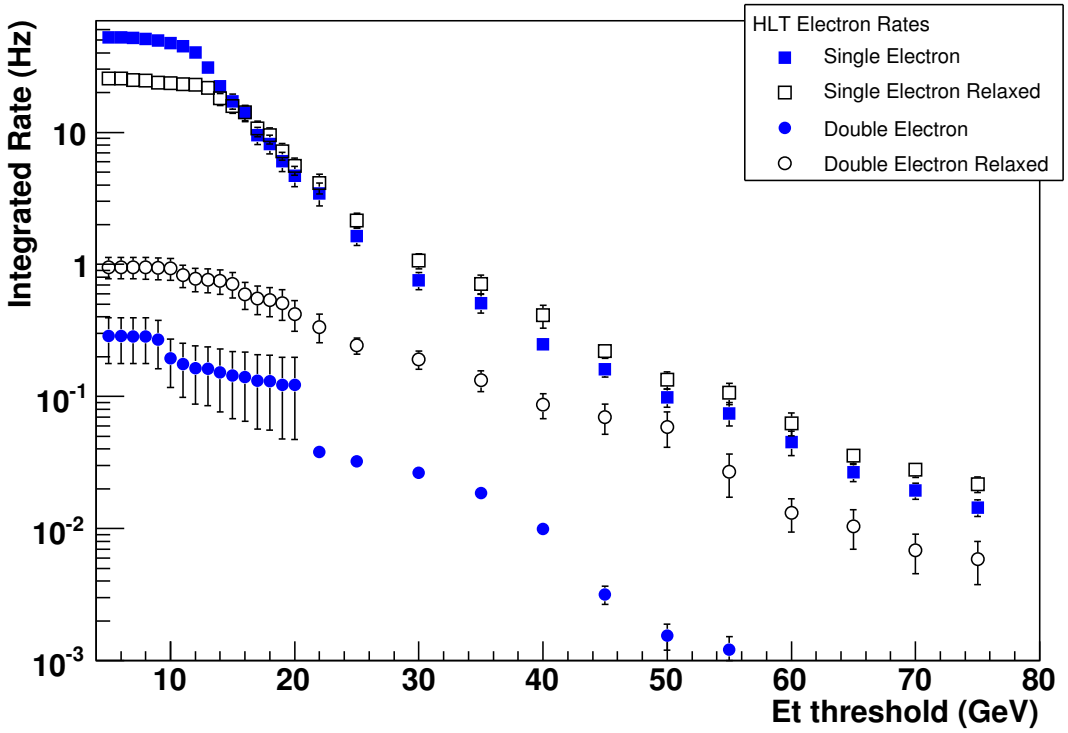

Figure 3.1: Electron HLT Rates versus E_T threshold.

Signal process	Isolated single photon	Relaxed single photon	Isolated double photon	Relaxed double photon
HLT: $H \rightarrow \gamma\gamma(m_H$=120 GeV)	80.5	76.8	75.8	75.7
L1*HLT: $H \rightarrow \gamma\gamma(m_H$=120 GeV)	78.8	76.8	58.7	72.7

Table 3.5: Signal efficiencies in % for photon HLT paths with and without folding in L1 efficiency.

3.3.3 CPU performance

The CPU time required for each step for single isolated electron path HLT reconstruction is shown in Table 3.7. The times listed are estimated using a sample of minimum-bias events which have accepted by the Level-1 trigger and which has been corrected for the fraction of events that pass any of the Level-1 EM trigger paths. The total mean time is 18.3 ms for this single electron path.

3.4 Prescaled Triggers

Prescaled Level-1 EM trigger paths with looser thresholds are included so that the efficiencies of the triggers in Table 3.1 can be measured. We allocate $\sim$ 5 Hz for these events. The thresholds and prescales applied at L1 are shown in Table 3.8. The thresholds and rates of the HLT prescaled trigger paths are shown in Table 3.9.

Signal process	single high energy EM	Single very high energy EM	Total
$Z' \to ee$ ($M \geq 200$ GeV)	67	7.0	67
$Z' \to ee$ ($M \geq 500$ GeV)	91	69	93
$Z' \to ee$ ($M \geq 1000$ GeV)	94	92	98
$Z' \to ee$ ($M \geq 2000$ GeV)	90	97	98
$G \to \gamma\gamma$ ($M \geq 2000$ GeV)	91	97	98

Table 3.6: Signal efficiencies in % for the high energy EM HLT paths. L1 efficiency is $\sim 100\%$.

HLT step	Running time (ms)	Averaged time (ms)	Fraction of all L1 events processed
ECAL unpacking	3.4	3.4	0.150
ECAL RecHits	2.8	2.8	0.150
ECAL clustering	2.8	2.8	0.150
HCAL unpacking	0.6	0.2	0.054
HCAL RecHits	1.1	0.4	0.054
HCAL isolation	0.5	0.2	0.054
Pixel unpacking	1.4	0.4	0.047
Pixel RecHits	1.8	0.6	0.047
Pixel clustering	4.2	1.3	0.047
Pixel seeding	3.1	1.0	0.047
SiStrip raw to clustering	0.2	0.0	0.003
Electron tracking	54.1	1.2	0.003
Track reconstruction for track isolation	228.0	4.0	0.003

Table 3.7: Processing times for the single electron path HLT reconstruction modules. The average times are obtained by scaling down the running times by the rejection obtained at various HLT levels.

Level-1 EM trigger path	Prescale	E_T threshold (GeV)
Single isolated	100	10
Single relaxed	100	10

Table 3.8: E_T thresholds for Level-1 EM prescaled trigger paths.

HLT trigger path	E_T threshold (GeV)	Rate(Hz)
Single isolated electron prescaled	11	0.3
Single isolated photon prescaled	12	2.5
Single relaxed photon prescaled	12	2.5

Table 3.9: E_T thresholds and rates for HLT EM prescaled trigger paths.

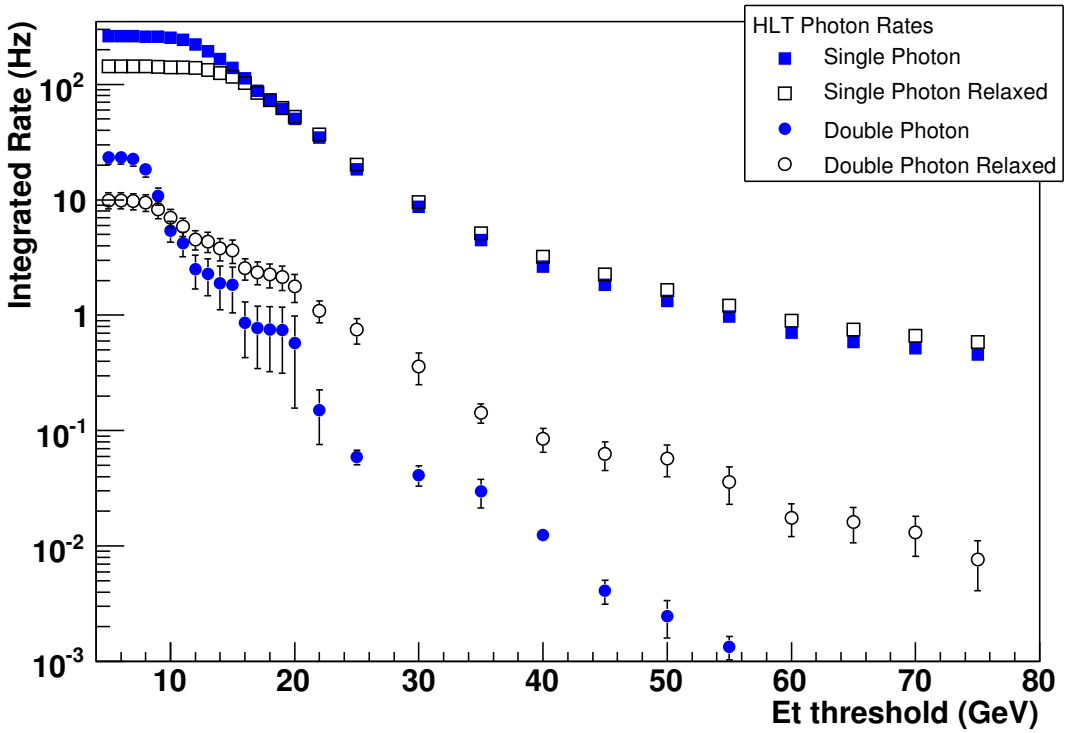

Figure 3.2: Photon HLT Rates versus E_T threshold.

Chapter 4

Triggers for Jets and Missing Transverse Energy

Measurements of the inclusive jet cross section, the dijet mass spectrum and the dijet angular distribution at the Tevatron have firmly established QCD as the fundamental model of the strong interaction. Some extensive QCD studies are therefore expected to be carried out at the LHC as well, especially since new physics may well manifest itself in deviations of QCD-dominated distributions from the standard model predictions. Indeed, many of the event signatures from SUSY, Higgs boson production, and other new physics processes include jets and/or $\not\!\!E_T$ in the final state.

In this chapter, we describe the HLT Jet and $\not\!\!E_T$ trigger paths for the startup physics run. Trigger rates and efficiencies for several of the jet and $\not\!\!E_T$ paths, along with the corresponding CPU requirements are shown.

4.1 Level-1 Trigger

Level-1 jets are defined using the transverse energy sums in 12×12 calorimeter trigger tower windows. A calorimeter trigger tower is defined as an array of 5×5 crystals in the ECAL of dimensions 0.087×0.087 ($\Delta\eta \times \Delta\phi$), which corresponds 1:1 to the physical tower size of the HCAL. The algorithm uses a sliding-window technique that steps in units of 4×4 trigger towers, called trigger regions, to give complete (η, ϕ) coverage of the calorimeter. The four highest jets in the central and forward calorimeters, as well as four central τ jets (Chapter 5) are selected. Also selected are single, double, triple and quad-jet triggers with varying thresholds and prescale factors.

The Level-1 $\not\!\!E_T$ trigger is calculated from the sum of the x and y components of the energy deposited in each trigger region. The $\mathrm{E_x}$ and $\mathrm{E_y}$ components are calculated using the coordinates of the center of the region. As with the jets, several $\not\!\!E_T$ triggers are possible depending on the threshold and prescale factor. A complete description of the jet and $\not\!\!E_T$ trigger algorithms at Level-1 is given in [4].

4.2 HLT algorithms for Jet and $\not\!\!E_T$ reconstruction

At HLT, jets are reconstructed using an iterative cone algorithm with cone size $R = 0.5$. The algorithm is identical to the one used in the offline analysis. The inputs to the jet algorithm are calorimeter towers, which are constructed from one or more projected HCAL cells and corresponding projected ECAL crystals, and satisfy certain threshold requirements. For in-

clusion in the jet finding algorithm, the calorimeter towers must have $p_T > 0.5$ GeV and at least one tower must satisfy the jet seed requirement of $p_T > 1$ GeV. After jet finding, a correction for the calorimeter response is applied to the reconstructed jets. This correction was obtained using QCD di-jet events generated by PYTHIA and run through the full CMS detector simulation in CMSSW.

As is the case with jet reconstruction, $\not\!\!E_T$ is calculated with the same algorithm used offline. The kinematic quantities associated with $\not\!\!E_T$ are calculated using calorimeter towers with the $p_T > 0.5$ GeV. No energy corrections are applied to the $\not\!\!E_T$ quantities at HLT. Detailed information regarding the jet and $\not\!\!E_T$ reconstruction algorithms, as well as the methodology used to determine the corrections for the calorimeter response, can be found in [9].

4.3 HLT performance

4.3.1 Trigger rates

Four single-jet trigger paths are proposed for the startup physics run. The p_T thresholds for these paths are 200, 150, 110, and 60 GeV. The Level-1 thresholds for these paths are chosen such that the Level-1 efficiency is at least 95% at the corresponding HLT threshold[1]

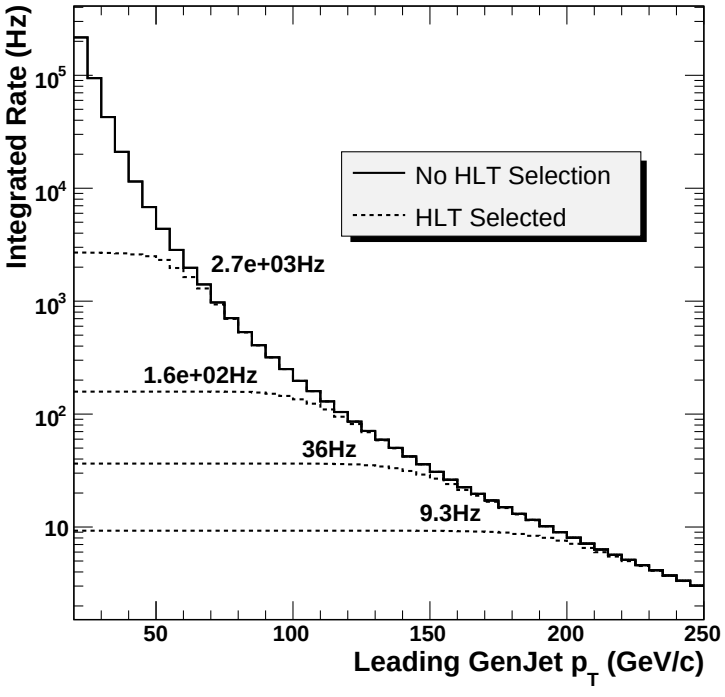

Figure 4.1: HLT rates for single-jet triggers as a function of generated jet p_T for $\mathcal{L} = 10^{32}\,\mathrm{cm}^{-2}\,\mathrm{s}^{-1}$. The solid curve has no Level-1 requirement, while the dashed curves have the Level-1 requirements for the single-jet trigger paths applied.

The path with the highest threshold is unprescaled and is designed to have an output rate of ~ 10Hz. The paths with lower thresholds are prescaled either at Level-1 or at the HLT to

[1]More detailed studies are presented at the Appendix of Ref. [5].

give output rates of order several Hz and to sustain a total single-jet output rate of about 15 Hz. Figure 4.1 shows the single-jet rates for $\mathcal{L} = 10^{32}\,\mathrm{cm}^{-2}\,\mathrm{s}^{-1}$ as a function of generated jet p_T. A more complete description of the design of the single-jet trigger menu is given in [10].

In addition to the single-jet paths, double, triple, and quad-jet triggers with p_T thresholds of 150, 85 and 60 GeV/c, respectively, are defined. The thresholds for these trigger paths chosen to given rates similar to the rates from the single-jet paths.

A $\not\!\!E_T$ path with threshold of 65 GeV/c has also been included, as well as multiple paths which require $\not\!\!E_T$ in combination with one or more jet paths. Event rates for jet plus $\not\!\!E_T$ triggers at a function of $\not\!\!E_T$ for four different jet p_T thresholds are shown in Figure 4.2.

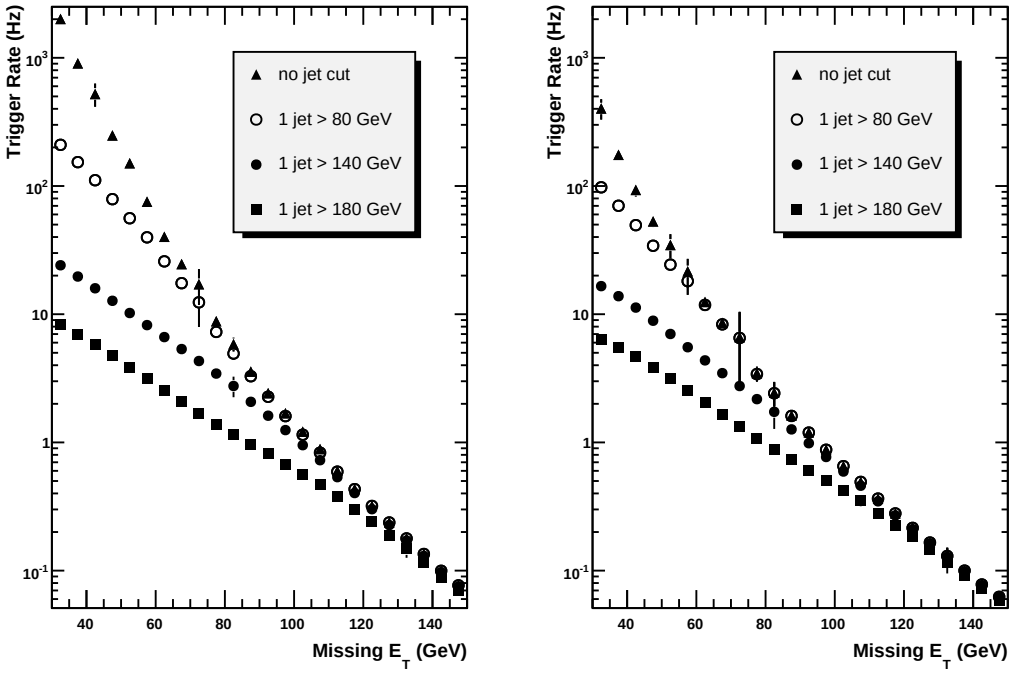

Figure 4.2: Event rates for jet plus $\not\!\!E_T$ triggers as a function of $\not\!\!E_T$, for *(left)* no Level-1 requirement, and *(right)* Level-1 $\not\!\!E_T > 30$ GeV.

Lower p_T thesholds for di-jet and jet + $\not\!\!E_T$ paths are obtainable by requiring an additional acoplanarity cut between the objects of interest. In the JetMET table, we define two such paths, one di-jet and one jet + $\not\!\!E_T$, with acoplanarity requirement $|\Delta\phi < 2.1|$.

The JetMET table also includes a specialized trigger path for Higgs produced via vector boson fusion (VBF) and two additional paths optimized for Susy searches. The VBF trigger is intended for Higgs boson events produced in $qq \to qqH$ process with the leading two jets in the final state satisfying the following "VBF conditions":

$$p_T^{j1}, p_T^{j2} > 40\,\mathrm{GeV}; \quad \eta_{j1} \times \eta_{j2} < 0 \quad \Delta\eta_{j1,j2} > 4.2$$

The full trigger menu of the proposed HLT paths for jet and $\not\!\!E_T$ for $\mathcal{L} = 10^{33}\,\mathrm{cm}^{-2}\,\mathrm{s}^{-1}$ is shown in Chapter 8.

4.3.2 Efficiency

Figure 4.3 displays the efficiency as a function of the jet E_T for different values of the HLT threshold.

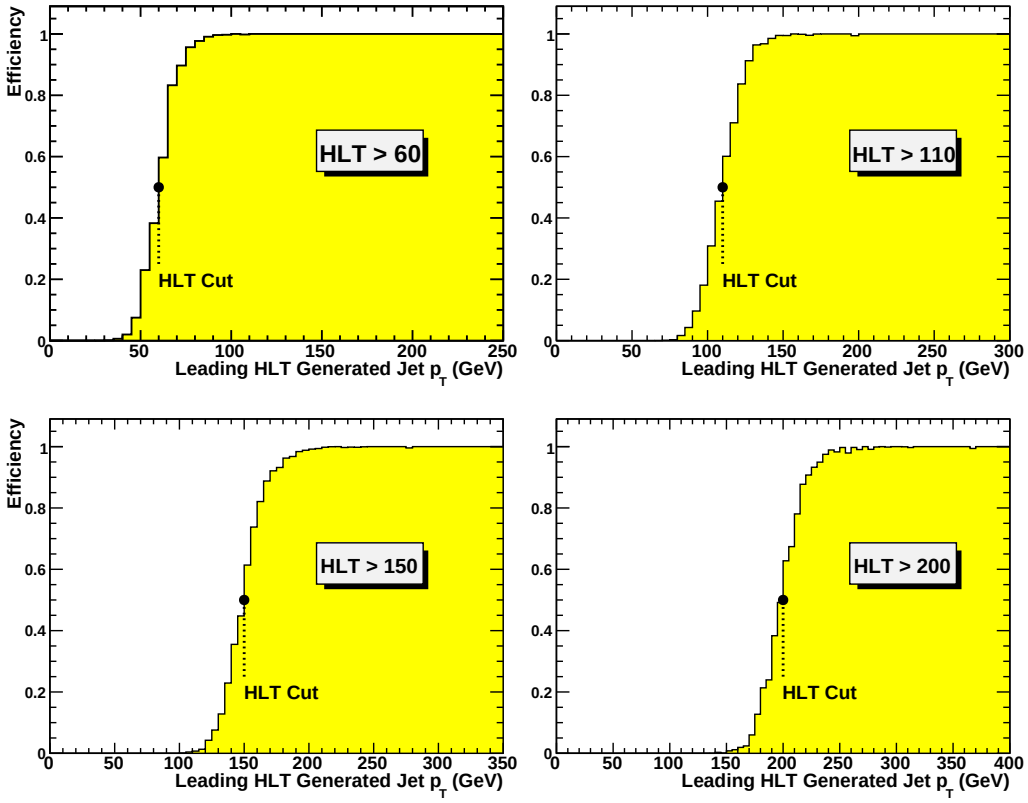

Figure 4.3: Turn-on curves for single jet triggers at HLT as a function of generated jet p_T.

The efficiency for the VBF trigger depends on the Higgs decay mode as well as the Higgs boson mass. In particular, for a Higgs boson decaying invisibly, the event is characterised by large $\not\!\!E_T$ and no hadronic or leptonic activity in the central region. The efficiencies for a Higgs boson mass of 200 GeV are 79%, 58% and 49% at L1 for a requirement of $\not\!\!E_T$ above 30, 50 and 60 GeV respectively. At HLT, the minimum $\not\!\!E_T$ requirement is 60 GeV. Subsequently, the HLT VBF condition is applied as specified above. The efficiencies are shown in Table 4.1. The events passing offline selection have HLT efficiency of 100%.

Table 4.1: Absolute Efficiency (%) for invisible higgs signal in VBF process, defined with respect to the number of generated events.

Higgs mass (GeV)	L1 Trigger	HLT	
	$\not\!\!E_T > 30$ GeV	$\not\!\!E_T > 60$ GeV	$\not\!\!E_T$ + VBF
200	79.1	51.5	8.5
160	77.8	48.7	7.0

4.3.3 CPU performance

CPU timing studies were performed using minimum-bias events and were cross-checked using QCD di-jet samples that were weighted to reproduce the expected jet trigger rates. Table 4.2 lists the average processing times for the various JetMET reconstruction procedures.

Procedure	Processing Time (ms)
ECAL Unpacking	14.6
ECAL RecHits	9.5
HCAL Unpacking	0.7
HCAL RecHits	1.5
Tower Maker	5.2
Jet Reco (ICONE5)	0.5
MET Reco	0.1

Table 4.2: Average processing times for the JetMET reconstruction procedures.

Chapter 5

Triggers for hadronic tau decays

Final states with hadronic tau decays (hereafter called *tau jets*) are an important signature in the search for Higgs bosons or for Supersymmetry. Because tau jets do not, by definition, contain leptons which could pass the corresponding Lvl-1 trigger requirements, specific triggering algorithms have to be developed both at Level-1 and HLT. In this Chapter, the Level-1 trigger conditions are first summarized in Section 5.1, followed by a brief account of the HLT algorithms and then physics performance and timing in Section 5.2.

5.1 Level 1 Trigger

A detailed description of the purely calorimetric Level-1 tau trigger can be found in Ref. [1]. A Level-1 jet is classified as a tau jet if the active trigger towers are confined in a 2×2 contiguous-trigger-tower array, in each of the 3×3 calorimeter regions (made of 4×4 trigger towers each). This criterion ensures both the narrowness and the isolation of the tau jet. Transverse energy thresholds are then applied to these energy deposits so as to reduce the trigger rates to an adequate level, *via* the definition of three paths,

- `SingleTau` path: $E_T > 80\,\text{GeV}$ for the largest transverse energy deposit;
- `DoubleTau` path: $E_T > 40\,\text{GeV}$ for the largest two transverse energy deposits;
- `TauWithMET` path: $E_T > 30\,\text{GeV}$ and $\not\!\!E_T > 30\,\text{GeV}$;

whose efficiency for a number of benchmark final states with taus is given in Table 5.1. The efficiency is the fraction of events generated with tau(s) selected by a given trigger path. The rates are given for QCD events in the $\hat{p_T}$ bin ranging from 30 and 170 GeV/c. Detailed information on the Level-1 efficiency is shown in the Appendix of Ref. [5].

Table 5.1: Efficiencies and rates for Level-1 tau trigger paths.

Samples/Trigger	SingleTau	DoubleTau	SingleTauMET
	Eff.	Eff.	Eff.
$Z \to \tau\tau$	19.6%	39%	39%
$W \to \tau\nu$	6%	–	18.5%
$H^{\pm} \to \tau\nu$ ($m_H = 200$ GeV/c^2)	68%	–	83%
$H^{\pm} \to \tau\nu$ ($m_H = 400\,\text{GeV/c}^2$)	76%	–	90%
Rate for QCD	680 Hz	2360 Hz	1960 Hz

5.2 HLT algorithms

5.2.1 General strategy

Reconstruction in the HLT is carried out in three steps (called, respectively, Level-2, Level-2.5 and Level-3 triggers), of increasing complexity and sophistication, so as to reject as many background events as possible before time-consuming algorithms are run while a high signal efficiency is retained, and to fulfill the performance prerequisites of the data acquisition.

The Level-2 algorithm relies only on calorimeter information. The Level-1 tau jets are used as seeds for regional calorimetric jet reconstruction with the iterative-cone algorithm and a cone radius R of 0.5 in the (η, ϕ) plane. Only jets with transverse energy in excess of 15 GeV passing isolation criteria are kept. The isolation requirement is that the sum of the transverse energy deposits in the ECAL, in an annulus $0.13 < R < 0.4$ around the jet direction, be smaller than 5 GeV.

The Level-2.5 and Level-3 algorithms use charged particle tracks reconstructed either with pixel hits only (fast, but terse, reconstruction), or with additional silicon-strip hits (slow, but accurate, reconstruction). The only difference between pixel and silicon-strip tracking is in the actual seeding of the track reconstruction, in the sense that the pixel tracking is done globally, with a lower p_T cut of 1 GeV/c, while a regional seeding is performed for the silicon-strip tracking, as follows.

- At Level-2.5, only seeds from pixel hits found in a small rectangle ($\Delta\eta$ = $\Delta\phi$ = 0.1) around the jet direction, and reconstructed with a p_T larger than 5 GeV/c are considered for tracking;
- At Level-3, the small rectangle is extended to $\Delta\eta$ = $\Delta\phi$ = 0.5 and the p_T cut is reduced to 1 GeV/c.

To reduce CPU usage, track reconstruction with silicon-strip hits is stopped when seven hits are found, at which point the momentum resolution is very close to that of the complete reconstruction. Reconstructed tracks are associated to a calorimetric jet if they are found in cone of radius 0.5 around its direction, and originate from the primary vertex, determined with pixel tracks only and associated with the largest transverse momentum sum.

Any of the three sets of tracks (globally seeded pixel tracks with $p_T > 1$ GeV/c, or silicon-strip tracks seeded in the small rectangle, with $p_T > 5$ GeV/c, on the one hand, and in the larger rectangle, with $p_T > 1$ GeV/c, on the other) may then be subjected to the following isolation algorithm. The tracks found in a cone of radius R=0.1 around the jet direction are called tau tracks. For the tau to be selected, the leading tau track must have a p_T larger than 3 GeV/c, and there must be no reconstructed tracks in an annulus $0.07 < R < 0.3$ around the leading tau track. More details can be found in Ref. [11].

5.2.2 HLT performance

5.2.2.1 Trigger rates & efficiency

Heavy charged Higgs bosons decaying to $\tau\nu$ lead to a single tau and missing energy. To reduce the rate of the `SingleTau` Level-1 path designed for this purpose, the calorimetric $\not\!\!E_T$ is required to exceed 65 GeV at level 2, and the leading track, reconstructed with silicon-strip hits, must have a p_T larger than 20 GeV/c at level 2.5 and the isolation annulus is extended to R<0.4. These criteria provide a final rate of $\sim$0.20$\pm$0.02 Hz, which allows the DAQ prereq-

uisites to be met. Efficiencies, computed with respect to the events that pass the `SingleTau` Level-1 trigger path are displayed in Table 5.2 for the successive steps of the HLT algorithms.

Table 5.2: Efficiencies and rates of the `SingleTau` HLT path.

	$H^{\pm} \rightarrow \tau\nu$		QCD
	M_H = 200 GeV/c^2	M_H = 400 GeV/c^2	$\hat{p_T}$ 120-170
Level-2 $\not\!\!E_T$ cut	59%	81%	6%
Level-2 Jet Reconstruction and Ecal Isolation	81%	85%	53%
Level-2.5 SiStrip Isolation	67%	76%	27%
Level-3 SiStrip Isolation	70%	72%	18%
HLT	23%	38%	0.15%
L1 * HLT	16%	29%	-

The `TauWithMet` Level-1 trigger path is designed specifically for the selection of $W \rightarrow \tau\nu$ events, with moderate requirements on the tau and missing transverse energies. In addition to the general isolation algorithms described in Section 5.2.1, these requirements are refined *(i)* at level 2, with an additional lower cut on the calorimetric $\not\!\!E_T$ of 35 GeV, and *(ii)* at level 2.5, by tightening the leading tau track p_T cut to 15 GeV/c and the isolation annulus is extended to $0.065 < R < 0.4$. These criteria provide a final rate of 1.84±0.2 Hz, which allows the DAQ prerequisites to be met. Efficiencies, computed with respect to the events that pass the `TauWithMET` Level-1 trigger path are displayed in Table 5.3.

Table 5.3: Efficiencies of the `TauWithMET` HLT path.

	$W \rightarrow \tau\nu$	QCD $\hat{p_T}$ 120-170
Level-2 $\not\!\!E_T$ cut	53%	35%
Level-2 Jet Reconstruction and Ecal Isolation	78%	57%
Level-2.5 SiStrip Isolation in the small rectangle	37%	30%
Level-3 SiStrip Isolation in the final rectangle	61%	20%
HLT	10%	1.2%
L1 * HLT	1.8%	-

Due to the presence of two taus, the general strategy described in Section 5.2.1 with global pixel tracking only is enough to meet the DAQ prerequisites, without the need for any additional requirements. Efficiencies for $Z \rightarrow \tau^+\tau^-$, computed with respect to events passing the Level-1 `doubleTau` trigger path are shown in Table 5.4, for the successive steps of the HLT algorithms. The total QCD rate is 4.95±0.65 Hz.

Table 5.4: Efficiencies and rates of the `DoubleTau` HLT path.

	$Z \rightarrow \tau\tau$	QCD $\hat{p_T}$ 120-170
Level-2 jet reconstruction	91%	58%
Level-2 Ecal Isolation	86%	37%
Level-2.5 Pixel Isolation	28%	0.77%
HLT	22%	0.17%
L1 * HLT	8.6%	-

5.2.2.2 CPU performance

The timing figures of the `TauWithMET` High-Level trigger path are shown in this section as a characteristic example. At level 2, the raw calorimeter data must be unpacked, and hits must be reconstructed around the L1 tau seeds. Calorimetric towers (with ECAL and HCAL information) are then built to proceed with jet reconstruction. For those events that pass the level 2 criteria, the pixel information must be unpacked, and clusters, hits and tracks have to be reconstructed. A similar chain is followed, when needed, with the silicon-strip information, all the way to track reconstruction. The time spent on average in each of these steps for minimum-bias events is displayed in Table 5.5. The silicon strip unpacking time is included in the track reconstruction.

Table 5.5: Timing for the `TauWithMet` High-Level trigger path.

HLT step	Running time (ms)	Averaged time (ms)	Fraction of all Level-1 events processed
ECAL unpacking	13.6	13.6	0.11
ECAL RecHits	9	9	0.11
HCAL unpacking	1	1	0.11
HCAL RecHits	3	3	0.11
Tower maker	4.5	4.5	0.11
Jet reconstruction	3	3	0.11
Pixel unpacking	2	0.1	0.006
Pixel clustering	6	0.3	0.006
Pixel recHits	2	0.1	0.006
Pixel Tracks	10	0.5	0.006
L2.5 Regional Seeding	11	0.5	0.006
L2.5 track reconstruction	60	2.7	0.006
L3 Regional Seeding	26	0.2	0.0008
L3 track reconstruction	280	2.0	0.0008
Total	421	41.5	

The first number (Running Time) is the time needed for an event to be processed through the corresponding step, while the second number (Averaged Time) refers to the time spent on average per minimum-bias event passing the Level-1 selection. (Many of these events are rejected early in the chain, thus reducing substantially the average time needed in the later steps.)

As anticipated earlier in this chapter, it can be noticed that the silicon-strip step absolute contribution is largest. Because the `SingleTau` cuts are intrinsically severe, and because no use is made of silicon-strip tracks in the `DoubleTau` path, the contribution of these paths to the overall timing is small.

Chapter 6

Triggers for b-jets

Many exotic physics channels contain b jets in the final state. By explicitly requiring b-tagged jets in an HLT path, one can use significantly lower jet energy thresholds than is possible for simple jet triggers (Section 4), increasing the trigger efficiency for these channels. Furthermore, events containing a μ associated with a jet can be used to measure the b-tag performance from data. This chapter describes two possible trigger paths that are tagged based on b-quark lifetime and semi-leptonic decays.

6.1 Level-1 Trigger

The b-lifetime HLT paths are all triggered at Level-1 by the jet or total-jet transverse energy triggers SingleJet150 .OR. DoubleJet100 .OR. TripleJet50 .OR. QuadJet30 .OR. HTT300.

The $b \rightarrow \mu$ HLT paths are all triggered at Level-1 by the muon and jet trigger Mu5_Jet15, with the exception of one HLT path (defined as bμp_tHLTpathHT in Sect. 6.2, which uses the total-jet transverse energy trigger HTT250 at Level 1.

Table 6.1: Performance of best Level-1 trigger paths. (N.B. The $t\bar{t}$ efficiencies quoted for the $b \rightarrow \mu$ trigger are obtained using events containing a generated μ).

L1 trigger name	Efficiency for hadronic $t\bar{t}$ events	Efficiency (Rate) for minimum bias events
b-lifetime		
SingleJet150	0.30	0.011×10^{-3} (0.07 kHz)
DoubleJet100	0.42	0.014×10^{-3} (0.11 kHz)
TripleJet50	0.84	0.028×10^{-3} (0.22 kHz)
QuadJet30	0.87	0.073×10^{-3} (0.58 kHz)
HTT300	0.91	0.082×10^{-3} (0.65 kHz)
.OR. of above	0.96	0.14×10^{-3} (1.1 kHz)
$\boldsymbol{b \rightarrow \mu}$		
Mu5_Jet15	0.74	0.51×10^{-3} (1.6 kHz)
HTT250	0.95	0.87×10^{-3} (2.56 kHz)

The performance of these Level-1 triggers on $t\bar{t}$ signal events and minimum bias background is listed in Table 6.1. One can deduce that the performance of the b-lifetime HLT would not in fact be significantly worse, (at least for $t\bar{t}$ selection), if it used only the QuadJet30 or the HTT300 triggers at Level-1.

6.2 HLT algorithms

Two varieties of HLT are studied, one using b-lifetime tagging (using the 'track-counting algorithm' and the other $b \rightarrow \mu$ tagging. Each consists of the following trigger thresholds (where the thresholds quoted are programmable):

- **b-lifetime HLT [12]:**
  - Level-2: Events are selected if they have 1, 2, 3 or 4 jets with p_t exceeding 180, 120, 70 or 40 GeV/c respectively. Alternatively, the event should have a transverse energy exceeding 470 GeV.
  - Level-2.5: Tracks are reconstructed using the Pixel Tracker alone (each with at least 3 hits), and are then used to reconstruct the primary vertex. The b-tag is run on the 4 highest E_t jets in the event with $E_t > 35$ GeV, using the pixel-tracks and primary vertex as input. It tags jets as b-jets if they have at least 2 tracks with a signed 3-D impact parameter significance $d_0/\sigma > 3.5$. Events pass if at least one jet is b-tagged.
  - Level-3: Tracks are reconstructed regionally in a cone of size $\Delta R = 0.25$ around jets tagged as b-jets at Level-2.5. The track reconstruction is partial, stopping after 8 hits have been assigned to a track. The b-tag uses these tracks and the primary vertex reconstructed at Level-2.5. It selects jets having at least 2 tracks with $d_0/\sigma > 6$. Events pass if at least one jet is b-tagged.

  The names of the b-lifetime based triggers are **bHLTpath1-4** or **bHLTpathHT** depending on which N-jet or HT trigger caused the event to pass Level-2.
- $\boldsymbol{b \rightarrow \mu}$ **HLT:**
  - Level-2: There are different selections for Level-2 jets available.
    1. One jet with $p_T > 20$ GeV/c.
    2. Two jets with $p_T > 120$ GeV/c.
    3. Three jet with $p_T > 70$ GeV/c.
    4. Four jets with $p_T > 40$ GeV/c.
    5. Event hadronic activity $H_T > 370$ GeV.
  - Level-2.5: Level-2 muons (see chapter 2), reconstructed using muon detector hits, are required to be near one of the Level-2 jets, $\Delta R(\mu - jet) < 0.4$, using the Soft Lepton b-tagging package.
  - Level-3: Further refinement to muons is provided by the use of tracking (see chapter 2). L3muons are used to select muon-in-jets by imposing the requirement $\Delta R(\mu - jet) < 0.4$. For some trigger paths, a further requirement $p_T(rel) > 0.7$ GeV/c on the Level-3 muons with respect to the jet axis is imposed.

  The names of the $b \rightarrow \mu$ based triggers are **bμp$_t$HLTpath2-4** or **bμp$_t$HLTpathHT** depending on which N-jet or HT trigger caused the event to pass Level-2. At Level-3, all these paths require $p_T(rel) > 0.7$ GeV/c. The exception is the path exploiting the 1-jet trigger at Level-2, which applies no $p_T(rel)$ cut. It is named **bμHLTpath1**.

  The bμHLTpath1 is designed to collect the muon-in-jet control samples for b-tagging performance studies. The other trigger paths, whose names begin with

bμp_tHLTpath, are used for particle searches, such as $t\bar{t}$ events with at least one muon.

6.3 HLT Performance

6.3.1 Trigger rates and efficiencies

In deciding the HLT requirements, one must bear in mind that about 5% of minimum bias events contain b quarks and therefore there is no point in achieving rejections higher than this. The trigger thresholds proposed in Sect. 6.2 are based on this fact. With these thresholds, b-tag HLT efficiencies for minimum-bias and hadronic $t\bar{t}$ events are given in Table 6.2.

Table 6.2: Performance of b-HLT trigger paths. (N.B. Efficiencies quoted relative to Level-1. Furthermore, the $t\bar{t}$ efficiencies quoted for the $b \rightarrow \mu$ trigger are obtained using events containing a generated μ).

b HLT trigger name	Efficiency for hadronic $t\bar{t}$ events	Efficiency (Rate) for minimum bias events	
b-lifetime			
bHLTpath1	0.045	0.0014	(1.5 Hz)
bHLTpath2	0.055	0.0022	(2.4 Hz)
bHLTpath3	0.13	0.0017	(1.9 Hz)
bHLTpath4	0.20	0.0019	(2.1 Hz)
bHLTpathHT	0.15	0.0026	(2.9 Hz)
.OR. of above	0.23	0.0045	(5.0 Hz)
$\boldsymbol{b \rightarrow \mu}$			
bμHLTpath1 prescaled by 20	n/a	0.82×10^{-3}	(2.4 Hz)
bμp_tHLTpath2	0.037	0.14×10^{-3}	(0.35 Hz)
bμp_tHLTpath3	0.06	0.64×10^{-4}	(0.16 Hz)
bμp_tHLTpath4	0.10	0.12×10^{-3}	(0.33 Hz)
bμp_tHLTpathHT	0.12	0.35×10^{-3}	(1.6 Hz)

Performance plots as a function of trigger thresholds are shown in the Appendix of Ref. [5].

In hard QCD events ($170 < \hat{p_t} < 230$ GeV/c), Levels 2.5 and 3 of the b-lifetime HLT keep 25% of the events containing b quarks and just 1.5% of the event containing only light quarks. Events containing b quarks make up 60% of the accepted events, so tightening the b-tag cuts further would achieve little. On individual jets, the L2.5 (L3) b-lifetime tagging can reject 80% (90%) of light quark jets whilst keeping 70% of b-jets [13].

In hard QCD events ($170 < \hat{p_t} < 230$ GeV/c), Levels 3 of the $b \rightarrow \mu$-HLT keeps 9% of the events containing b quarks and just 1% of the event containing only light quarks. Note that this includes the $b \rightarrow \mu$ decay branching fraction.

6.3.2 CPU performance

Table 6.3 shows the time taken by the slowest software modules, when running on a 3 GHz machine. Event unpacking time is not shown.

(For $b \rightarrow \mu$ HLT, the timing information was obtained by running on 1000 events from a minimum bias event skim which in addition required the presence of a muon in each event.)

Table 6.3: Running and average processing times for the slowest modules in the b-tag reconstruction.

HLT step	Running time (ms)	Averaged time (ms)	Fraction of all L1 events processed
b-lifetime HLT (total for all paths)			
ecalDigis	13	13	0.066
ecalWeightUncalibRecHit	7	7	0.066
towerMaker	5	5	0.066
pixelTracks	18	1	0.004
bJetregionalCkfTrackCandidates	300	4	0.001
$b \rightarrow \mu$ HLT (illustrated by bμp_tHLTpath2)			
ecalDigis	13	13	0.074
L2Muons	17	<1	<0.001
L3Muons	136	< 1	<0.001

6.3.3 b Calibration

The HLT b-tagging efficiency can be measured using $t\bar{t}$ events in which one or both top quarks decay semi-leptonically and one of the jets is tagged as a b-jet by the offline b-tagging algorithm.

For example, the performance of the $b \rightarrow \mu$ paths bμp_tHLTpath2-4 can be evaluated by selecting offline reconstructed $t\bar{t}$ events which pass the Muon-plus-Jet HLT and then estimating what fraction of these events pass the bμp_tHLTpath2-4 paths. The Level-1 trigger conditions for the HLT paths being compared are the same (A_Mu5_Jet15). In order to decouple the estimate of the performance of the $b \rightarrow \mu$ component from that of the Level-2 jet, one will need to enforce offline identical L2 jet requirements for the Muon-plus-Jet and the $b \rightarrow \mu$ HLT path under consideration.

In addition, one can select offline a pure sample of b-jets using the offline b-tagging algorithm, and check what fraction are tagged by the b-tagging algorithms used at HLT.

Chapter 7

Triggers on Combinations of Objects

The inclusion of triggers combining different physics objects, e.g. different lepton species (e and μ) or a lepton and a τ-jet allows for lowering the thresholds on the input physics objects, therefore increasing the eficiency for signals that involve these multiple objects.

As an example, the lepton+tau-jet trigger is motivated by searches for Higgs bosons and Supersymmetric particles. In the Standard Model, a Higgs boson can be produced via a vector boson fusion (qqH) and in SUSY via gluon fusion gg→bbA^0/H^0. In both cases, the Higgs boson can decay into two τ leptons which in turn can decay into either a lepton l = e, μ or hadronically forming a "τ-jet". The inclusion of dedicated lepton+tau-jet channels opens the possibility of increasing the efficiency for selecting these Higgs decays.

7.1 Muon + electron Triggers

Two HLT paths are built using combinations of electron and muon candidates with either isolated or relaxed criteria. They rely on the same Level-1 and HLT electron and muon reconstruction as the single electron and single muons paths. The two paths require:

1. Level-1 Accept by one of the three conditions: `A_Mu3_IsoEG5`, `A_Mu5_IsoEG10` or `A_Mu3_EG12`.
2. At least one HLT electron candidate fulfilling the criteria applied in the single electron path (Sec. 3.2), but with a lower E_T threshold.
3. At least one HLT muon candidate fulfilling the criteria applied in the single muon path, as described in Sec. 2.2.

In the first (isolated) path, the same isolation requirements are set on the electron and muon as in the "Single Isolated electron" and "Single isolated muon" paths, respectively. In the second (relaxed) path, the isolation requirements are dropped. The thresholds for the two HLT paths are listed in Table 7.1.

Table 7.1: Suite of electron-plus-muon HLT paths.

HLT Path	e E_T threshold	μ P_T threshold
Isolated e + μ	8 GeV	7 GeV
Relaxed e + μ	10 GeV	10 GeV

7.2 Lepton+tau-jet triggers

7.2.1 electron+tau trigger

At Level-1, the seed-bit A_ISOEG10_TAUJET20 (see Ch. 8) where ISOEG stands for an isolated electromagnetic object with $p_T^e \geq 10$ GeV/c and τ-jet with $p_T^\tau \geq 20$ GeV/c, is requested to fire. Both Level-1 `IsoEG` and τ-jet candidates are requested not to be colinear.

At the HLT, the $e + \tau$ trigger path consists in the following steps:

1. Reconstruction of the electron – which is fast in terms of cpu, and is caried up to the HLT following the standard isolated single electron reconstruction described in section 3.2.
2. Level-2 confirms the Level-1τ-jet candidates. This is achieved by running a jet-finder on the calorimeter towers associated with the four highest Level-1 jet candidates (see section 5). These Level-2 jets are requested to match the Level-1-tau jet candidates.
3. At Level-2.5, τ-jet candidates are selected from single-τ+X and double-τ candidates and required to be isolated. The isolation procedure is performed with regional tracking reconstruction (as in section 5.2.1).
4. Level-3 imposes further isolation criteria with larger reconstruction regions in order to achieve the desired QCD rejection factor.

A set of some of the main selection criteria applied at Level-1 and HLT are summariesed in Table. 7.2.

Selection Criteria	eτ jet + e Trigger Selections
Level-1 τ , IsoEG E_T [GeV]	20, 10
HLT e E_T [GeV]	12
L25 Regional pixel seeding region $\delta\eta, \delta\phi$	0.1, 0.1
L25 LeptonTau Cone Isolation ΔR_{iso}, ΔR_{sig}, P_T^{LdgTr}	0.45, 0.07, 6 GeV/c
L3 Regional pixel seeding region $\delta\eta, \delta\phi$	0.5 , 0.5
L3 LeptonTau Cone Isolation ΔR_{iso}, ΔR_{sig}, P_T^{LdgTr}	0.45, 0.07 , 6 GeV/c
Single IsoEG E_T [GeV]	12
Single Electron HLT E_T [GeV]	15

Table 7.2: Table summarising some of the eτ+e trigger selection criteria. None of these parameters has been fully tuned

7.2.1.1 HLT Performance

The signal considered is $Z \rightarrow \tau\tau \rightarrow e\tau-$jet with $|\eta_e| < 2.5$ and $|\eta_{\tau-\text{jet}}| < 2.5$. Fig. 7.1 displays the HLT efficiencies for selecting isolated electrons and τ-jets candidates as a function of their respective p_T for events that have passed the Level-1 requirements.

7.2.1.2 single-e .AND. $e + \tau$ trigger performance and rates

In order to achieve high signal selection efficiencies, events are selected using a combination of two triggers: a single isolated e/γ (ISOEG) and the previously described the $e + \tau$ trigger.In the following, it will be designated by "$e + e\tau$".

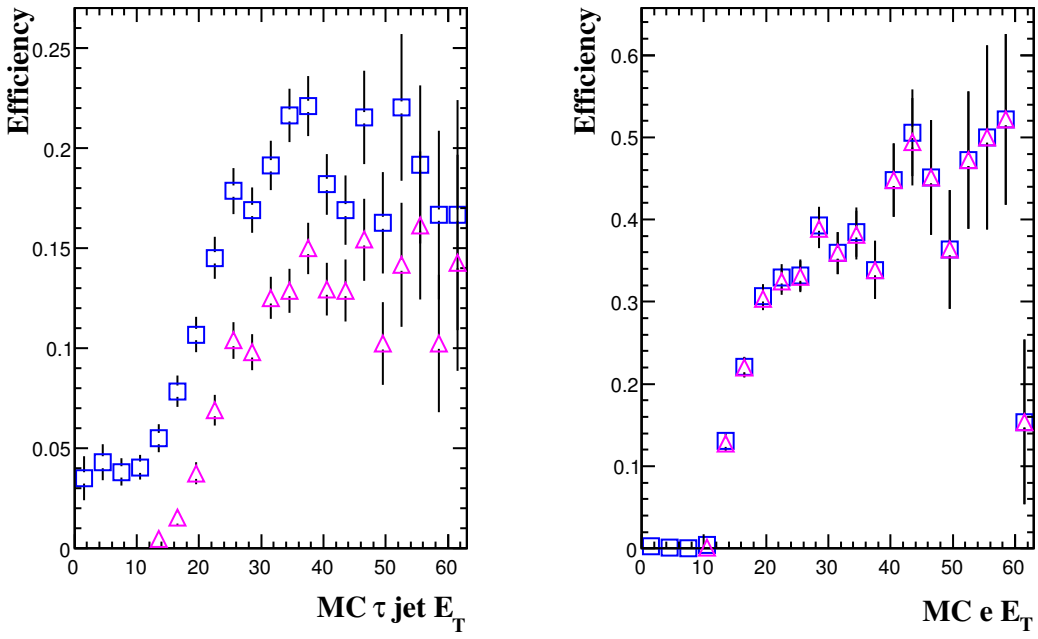

Figure 7.1: Turn-on curves for $Z \rightarrow \tau\tau \rightarrow e\tau-\mathrm{jet}$ events of the HLT electron from the $e+\tau$ trigger with τ $\mathrm{p_T} > 20$ GeV/c (left) and IsoEG $\mathrm{p_T} > 12$ GeV/c (right) thresholds. The triangle distributions require matching between the HLT and MC objects.

The threshold $\mathrm{p_T}$ for the single electron trigger is high ($\mathrm{p_T^e} \geq 15$ GeV/c) to suppress contamination from QCD jets and hence keep a high purity of the selected objects while satisfying the trigger rates requirements. In the case of the $e+\tau$ trigger ($\mathrm{p_T^e} \geq 10$ GeV/c), the threshold of the electron can be considerably lowered without decreasing the signal purity thanks to the topological constraint introduced by the requirements of an additional τ-jet in the event. This leads to a significant increase of signal selection efficency in the region of low $\mathrm{p_T^e}$ of the electron spectrum. Table 7.3 compiles the selection efficiencies and rates from Level-1 to HLT for both the $e+\tau$ and $e+e\tau$ trigger paths.

Trigger/Samples	$Z \rightarrow e+\tau$-jet	QCD $\hat{\mathrm{p}}_\mathrm{T}$ 15-170 GeV/c
Level-1 $e+\tau$	$(43.9 \pm 0.4)\%$	(1.92 ± 0.05) kHz
HLT $e+\tau$	$(30.2 \pm 0.6)\%$	(1.01 ± 0.5) Hz
Level-1 + HLT $e+\tau$	$(13.2 \pm 0.3)\%$	(0.13 ± 0.07) Hz
Level-1 $e+e\tau$	$(55.8 \pm 0.4)\%$	(3.15 ± 0.07) kHz
Level-1+HLT $e+e\tau$	$(24.5 \pm 0.4)\%$	(14.08 ± 3.58) Hz

Table 7.3: Level-1 and HLT efficiencies and rates of the $e+\tau$ and the combined $e+e\tau$ triggers. At Level-1 the E_T thresholds for the $e+\tau$ trigger are (10,20) GeV respectively and 15 GeV for the single-e trigger. At HLT the electron threshold of the $e+\tau$ trigger is set to 12 GeV and 15 GeV for the single-e trigger. Only $e-\tau$-jet non-collinear pairs are selected at Level-1 only. Rates are calculated at an LHC start-up luminosity $\mathcal{L} = 10^{32}$ cm^{-2} s^{-1}.

7.2.2 Muon+tau trigger

A dedicated Muon+Tau Level-1 trigger bit with a 5 GeV threshold on the muon transverse momentum and a 20 GeV threshold on the tau-jet transverse energy is also used.

In the first step of the HLT the standard Level-2 muon algorithm is run and events without a reconstructed muon with transverse momentum above 15 GeV are rejected. Next the tau jets are reconstructed in the calorimeter. If there is any isolated jet, which matches a Level-1 tau jet, the event is kept.

To further cut the background, the isolated jets are matched to pixel tracks and the cone isolation algorithm is applied. The leading track is required to have a transverse momentum of at least 3 GeV and the isolation cone size is set to 0.45 in order to sufficiently lower the background rate.

The final and most-time consuming step is the standard Level-3 Muon reconstruction. The event is required to have at least one isolated Level-3 Muon with transverse momentum larger than 15 GeV.

The efficiencies of all these steps are listed in table 7.2.2 for a signal sample of ($qqh(135) \rightarrow \tau_\mu\tau_h$) events along with a muon-enriched background (μX) sample. The purity of the qqh sample is 0.68 after the Level-1 trigger and 0.96 after the complete HLT. Figure 7.2 shows the HLT efficiency for a signal and a background sample as a function of the isolation cone size.

Table 7.4: Level-1 and HLT efficiencies of the Muon+Tau trigger.

Step	$qqh \rightarrow \tau_\mu\tau_h$	μX
Level-1 $\mu + \tau$	0.61	0.29
Isol. Level-2 μ	0.71	0.08
Ecal isolation	0.83	0.32
Pixel isolation	0.47	0.04
Isol. Level-3 μ	0.76	0.04
Total HLT	0.21	$5 \cdot 10^{-5}$

7.3 Electron-plus-Jet Triggers

7.3.1 Level-1 Trigger

Combined triggering on electrons and jet(s) (e+jet) allows for generic low-rate triggers on a number of physics processes, from $t\bar{t}$ production, to searches for SUSY in cascade decays. Requiring more than one jet in addition to the electron or requiring the electron not to be back-to-back with the jet allows for the control of rates both at Level-1 and HLT.

The Level-1 triggers used in this selection are listed in Table 7.5. Since the proposed triggers are geared for low-luminosity running, all of them require a single jet. Moreover, apart from the requirement of the electron Level-1 candidate to be more than ΔR away from the leading Level-1 jet candidate to avoid double counting, no further topological cuts are introduced. In this table the IsoEG trigger terms refers to an isolated EM object, while the EG term refers to either an isolated or a non-isolated EM object [1].

[1] As discussed previously, the Level-1 trigger is capable of finding up to four isolated and four non-isolated EM objects, with the two categories being mutually exclusive.

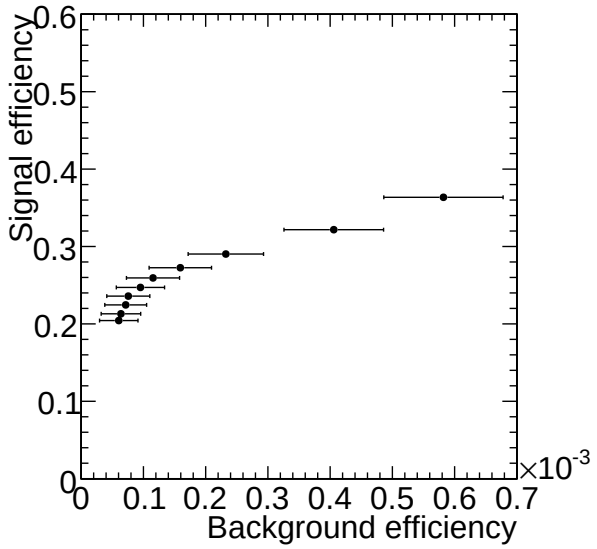

Figure 7.2: Efficiency of a signal ($qqh(135) \rightarrow \tau_\mu\tau_h$) vs. a background ($\mu X$) sample as a function of the isolation cone size. The isolation cone size is varied from 0.05 to 0.5 in steps of 0.05.

The thresholds for these triggers have not been thoroughly optimized yet. Nevertheless, the rate studies were performed in the plane of (Iso)EG and Jet-object thresholds, thus paving the way for a straightforward optimization of the thresholds for a given accept rate of the trigger. More detailed studies are discussed in the Appendix of Ref. [5].

The efficiencies of various triggers in the electron-plus-jet suite for the $t\bar{t}$ events and for several benchmark SUSY signal points (LM1, LM4, LM5, LM9) are summarized in Table 7.6.

The efficiencies of various triggers in the e+jet suite for the $t\bar{t}$ events and for several benchmark SUSY signal points (LM1, LM4, LM5, LM9). These efficiencies are summarized in Table 7.6. The only HLT e+jet trigger which has been included in this HLT exercise is HLT1XElectron1Jets trigger working off the A_IsoEG10_Jet30 Level-1 trigger with the thresholds of $p_T(e) > 12$ GeV, and $p_T(\text{jet}) > 40$ GeV.

Table 7.5: Suite of e+jet Level-1 triggers and the expected unprescaled rate.

Name	EM p_T threshold	Jet p_T threshold	Prescale	Rate at 10^{32} cm^{-2}s^{-1}
A_IsoEG10_Jet15	10 GeV	15 GeV	20	3.40 kHz
A_IsoEG10_Jet20	10 GeV	20 GeV	1	2.97 kHz
A_IsoEG10_Jet30	10 GeV	30 GeV	1	1.96 kHz
A_IsoEG10_Jet70	10 GeV	70 GeV	1	0.24 kHz
A_EG10_Jet15	10 GeV	15 GeV	20	4.37 kHz
A_EG12_Jet20	12 GeV	20 GeV	1	2.38 kHz
A_EG12_Jet70	12 GeV	70 GeV	1	0.34 kHz

7.3.2 HLT selection

Different electron+jets HLT paths are foreseen, which differ by the multiplicity of HLT jet candidates. So far, only the path electron $+\geq 1$ jet has been studied in detail. It requires:

- that the event be accepted by one of the Level 1 triggers listed in table 7.5.
- at least one HLT electron candidate fullfilling the criteria applied in the "single electron" path (see chapter 3.2): HCAL isolation cut, matching with hits in the pixel detector, isolation criterium with respect to neighbouring tracks, cut on the ratio of the super-cluster energy to the momentum of the associated track. The latter cut is relaxed for electrons in the barrel, requiring $E/p < 2$.
- at least one HLT jet candidates, reconstructed as described in chapter 4.

7.3.3 HLT performance

Figure 7.3 (left) shows the HLT rate of the electron $+\geq 1$ jet path as a function of the thresholds applied on the transverse momentum of the electron and jet candidates, for a luminosity of 10^{32} cm^{-2}s^{-1}. These rates are calculated on QCD Monte-Carlo events which fire the A_IsoEG10_Jet30 Level 1 trigger bit. The trigger efficiencies for $t\bar{t}$ events where at least one of the W bosons decays into an electron are shown in Fig. 7.3 (right). Figure 7.4 shows the HLT efficiency for events from the LM1 SUSY benchmark point.

Requiring that the $P_T(e) > 12$ GeV, and that the jet have $P_T > 40$ GeV, the expected rate is about 10 Hz. For these cuts, the HLT efficiency on $t\bar{t}$ events is about 64%. The efficiency for several benchmark SUSY signal points is given in the last line of Table 7.6.

7.4 Muon plus (b-)jet Triggers

The triggers described in this section use the HLT algorithms and filters defined in the muon and (b-)jet sections. Combined triggering on muons and jet(s) (μ+jet) allows for generic low-rate triggers on a number of physics processes, from standard model $t\bar{t}$ production to searches for SUSY in cascade decays. Requiring more than one jet in addition to the muon allows to control rates both at the Level 1 and at high-level trigger.

Table 7.6: Efficiency of e+jet Level-1 triggers for various physics processes. For the $t\bar{t}$ channel the efficiency is quoted for the e+jets final state. For SUSY points the first number is the efficiency given the presence of an electron in the decay chain and the second number in parenthesis is the overall efficiency. The efficiency for the HLT trigger is quoted on top of the corresponding Level-1 trigger (A_IsoEG10_Jet30) efficiency.

Name	$t\bar{t}$	LM1	LM4	LM5	LM9
A_IsoEG10_Jet15	83.3%	73.1% (15.4%)	84.8% (12.0%)	81.0% (8.83%)	79.8% (10.6%)
A_IsoEG10_Jet20	83.3%	72.8% (15.4%)	84.5% (11.9%)	81.0% (8.83%)	79.2% (10.5%)
A_IsoEG10_Jet30	83.2%	72.4% (15.3%)	84.3% (11.0%)	80.5% (8.77%)	76.7% (10.2%)
A_IsoEG10_Jet70	79.2%	71.0% (15.0%)	83.4% (10.6%)	79.0% (8.61%)	72.4% (9.61%)
A_EG10_Jet15	94.3%	86.4% (18.3%)	98.0% (13.7%)	96.3% (10.5%)	91.5% (12.1%)
A_EG12_Jet20	92.4%	82.2% (17.4%)	96.9% (13.9%)	95.0% (10.4%)	88.4% (11.7%)
A_EG12_Jet70	87.6%	80.6% (17.0%)	95.2% (13.0%)	92.7% (10.1%)	81.7% (10.8%)
HLT1XElectron1Jet	64%	63%	68%	63%	65%

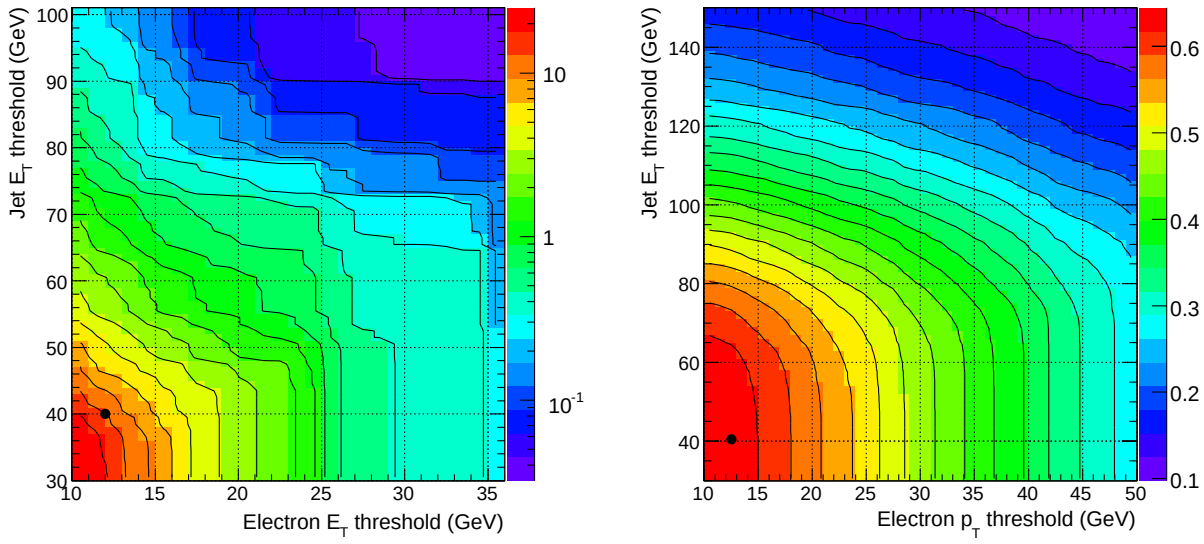

Figure 7.3: (left) HLT rate, in Hz, of the electron $+\geq 1$ jet path as a function of the thresholds applied on the transverse momentum of the electron and jet candidates. These are shown for a luminosity of of 10^{32} cm^{-2}s^{-1}. (right) Efficiency of the electron $+\geq 1$ jet HLT path on $t\bar{t}$ events.

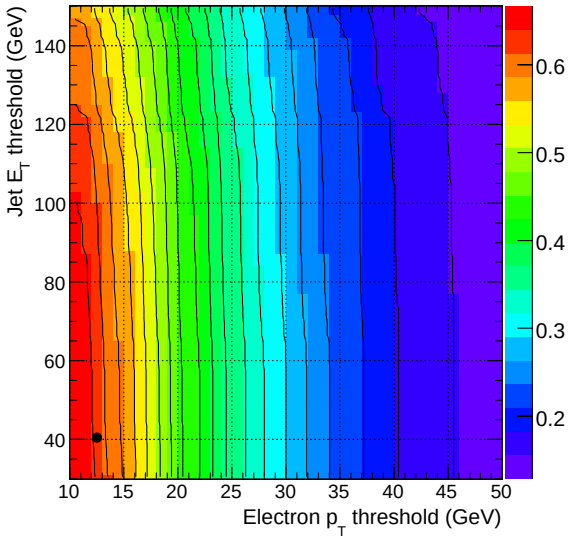

Figure 7.4: Efficiency of the electron $+\geq 1$ jet HLT path on events from the LM1 SUSY benchmark point.

7.4.1 Level-1 Trigger

The Level-1 triggers used are summarized in Table 7.7. Since the proposed triggers are geared for low-luminosity running, all of them only required a single jet.

Table 7.7: Suite of muon-plus-jet Level-1 triggers and the expected unprescaled rate at the instantaneous luminosity of 10^{32} cm^{-2}s^{-1}.

Name	Muon p_T threshold	Jet p_T threshold	Prescale	Rate at 10^{32} cm^{-2}s^{-1}
A_Mu3_Jet15	3 GeV	15 GeV	20	3.15 ± 0.21 kHz
A_Mu3_Jet70	3 GeV	70 GeV	1	0.10 ± 0.03 kHz
A_Mu5_Jet15	5 GeV	15 GeV	1	1.42 ± 0.13 kHz
A_Mu5_Jet20	5 GeV	20 GeV	1	1.05 ± 0.10 kHz

While the thresholds for these triggers have not been thoroughly optimized yet, careful rates studies have been performed in the plane of μ and Jet-object thresholds, which would allow for an easy optimization of the thresholds for a given accept rate of the trigger.

An important characteristic of the μ+jet triggers is the turn-on of both the muon and jet terms. For the turn-on studies, we used SUSY signal sample for benchmark points LM1, LM2, LM4, LM5, and LM9.

More detailed studies on rates and turn-on curves are discussed in the Appendix of Ref. [5].

The efficiency of the various Level-1 triggers in the μ+jet suite for $t\bar{t}$ events and for several benchmark SUSY signal points (LM1, LM4, LM5, LM9) are summarized in Table 7.8.

Name	$t\bar{t}$	LM1	LM4	LM5	LM9
A_Mu3_Jet15	91.1%	92.3% (19.5%)	94.6% (13.1%)	95.4% (10.5%)	91.2% (12.5%)
A_Mu3_Jet70	85.5%	88.4% (18.6%)	91.0% (12.6%)	93.0% (10.2%)	83.0% (11.4%)
A_Mu5_Jet15	84.4%	86.0% (18.1%)	89.3% (12.3%)	91.7% (10.1%)	86.1% (11.8%)
A_Mu5_Jet20	84.3%	85.2% (18.0%)	89.1% (12.3%)	91.7% (10.1%)	85.5% (11.7%)

Table 7.8: Efficiency of muon-plus-jet Level 1 triggers for various physics processes. For the $t\bar{t}$ channel the efficiency is quoted for the muon-plus-jets final state. For SUSY points the first number is the efficiency given the presence of a muon in the decay chain and the second number in parenthesis is an overall efficiency.

7.4.2 Muon-plus-Jet HLT

The HLT path consists of the combination of isolated muon and jet paths. It requires:

1. that the event have been accepted by the Level 1 trigger bit A_Mu5_Jet15.
2. at least one HLT muon candidate, defined as a track found by the Level-2 muon standalone reconstruction that satisfies level-2 calorimetry isolation criteria and that can be combined through global reconstruction with a track in the central tracker, where Level-3 track isolation is also required.
3. at least one HLT jet candidate, reconstructed as described in chapter chapter 4

The HLT background rate for this trigger was evaluated using both the muon-enriched sample described in section 2.2.1 and using minimum-bias events containing at least one prompt muon above 3 GeV and QCD generated samples. Both methods yield compatible results, shown in figure 7.6 for the muon enriched sample. The chosen startup jet and muon p_T thresholds are 7 and 40 GeV respectively, yielding a rate of 4.2 Hz for the muon-enriched sample, in reasonable agreement with the value of 5.0 Hz obtained on QCD samples and minimum bias events selected to contain prompt muons with p_T above 3 GeV. The corresponding efficiencies for $t\bar{t} \rightarrow \mu + jets$ and SUSY benchmark points are summarized in table 7.9.

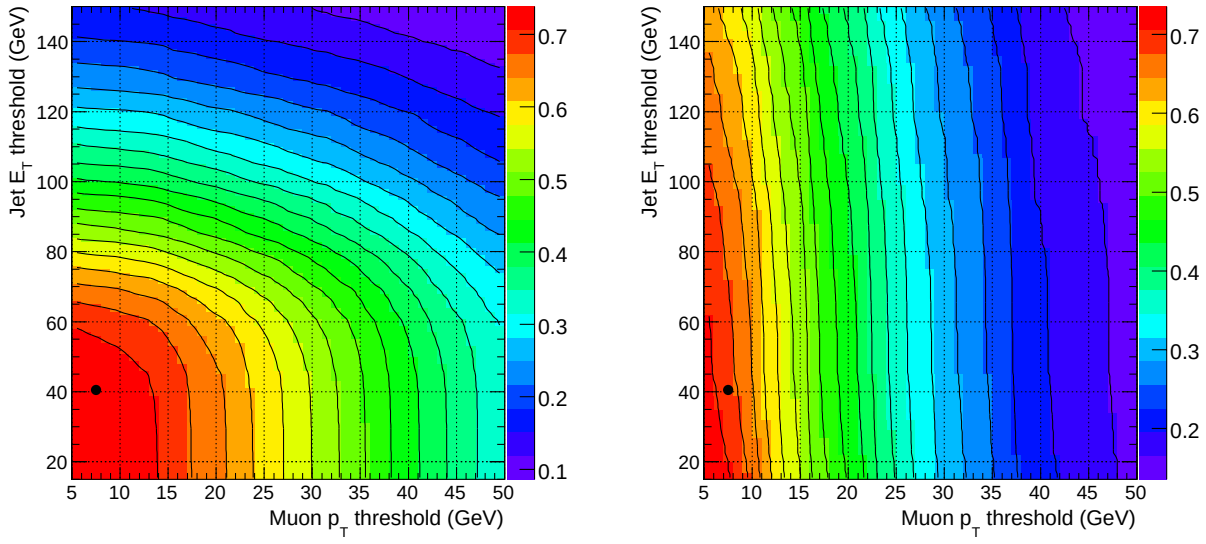

Figure 7.5: HLT efficiency of the muon-plus-jet path for $t\bar{t} \rightarrow \mu + jet$ events (left) and SUSY LM1 benchmark point (right) as a function of jet and muon thresholds.

Name	$t\bar{t} \rightarrow \mu + jets$	LM1	LM4	LM5	LM9
Muon (7 GeV) + jet (40 GeV)	73%	69%	71%	72%	68%
Muon (7 GeV) + b-jet (35 GeV)	24%	16%	22%	22%	16%

Table 7.9: HLT Efficiency of muon-plus-(b)jet per L1-accepted event with the A_Mu5_Jet15 bit, for various physics processes. For the $t\bar{t}$ channel the efficiency is quoted for the muon-plus-jets final state. For SUSY points the first number is the efficiency given the presence of a muon in the decay chain.

7.4.3 Muon plus b-jets HLT

The HLT path consists of the combination of isolated muon and b-tag paths. As the muon HLT steps do not require the tracker information before level-3, these rejection steps are run first. The HLT path can be summarized as follows.

1. Level 1 accept with trigger bit A_Mu5_Jet15
2. Level-2 reconstruction and isolation of the muon

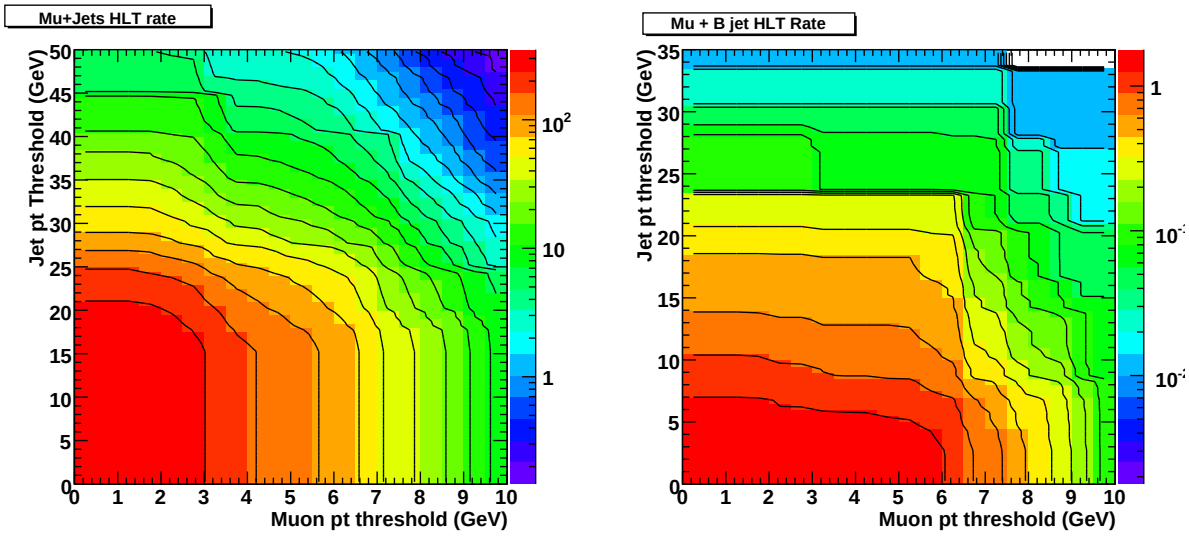

Figure 7.6: HLT rate for the muon-plus-jet (left) and muon-plus-bjet (right) HLT trigger, based on the muon enriched sample as a function of jet and muon thresholds at the instantaneous luminosity of 10^{32} cm^{-2}s^{-1}.

3. Level-2 calorimeter based jet reconstruction for b-tag and selection based on p_T (minimum 35 GeV)
4. Level-2.5 pixel track reconstruction within the jet region and lifetime b-tag
5. Level-3 reconstruction and pixel isolation of the muon
6. Level-3 b-tag: silicon strip tracker track reconstruction in the jet region and track-counting b-tagging.

Figure 7.6 shows a clearly negligible rate (0.015 Hz) at startup luminosity for the p_T cut of 35 GeV applied on the b-jet. The corresponding signal efficiencies for $t\bar{t} \rightarrow \mu + jets$ and SUSY benchmark points are summarized in table 7.9 and shown in figure 7.7, showing only a factor 3 reduction with respect to the mu+jet path, for much lower background rates.
The average time taken by this path is 2.3 ms per Level 1-accepted event on a 3 GHz Dual Core Intel Xeon computer running SLC4.

7.5 Other Triggers

7.5.1 Trigger for displaced J/ψ's

This trigger is mainly useful for b-Physics studies. Many channels of interest contain two muons in the final state. Many of these muon-pairs originate from J/ψ's, like in the decays $B_s \rightarrow J/\psi\phi$, $B^+ \rightarrow J/\psi K^+$ or $B_d \rightarrow J/\psi K^*$

At Level-1 the Dimuon Level-1 trigger with a threshold of 3 GeV/c is used.

7.5.1.1 HLT selection of non-prompt J/ψ's

In the first step, this trigger is similar to the di-muon trigger (see chapter 2), where the same Level-2 muons candidates are used. At least two muons with opposite charge and transverse

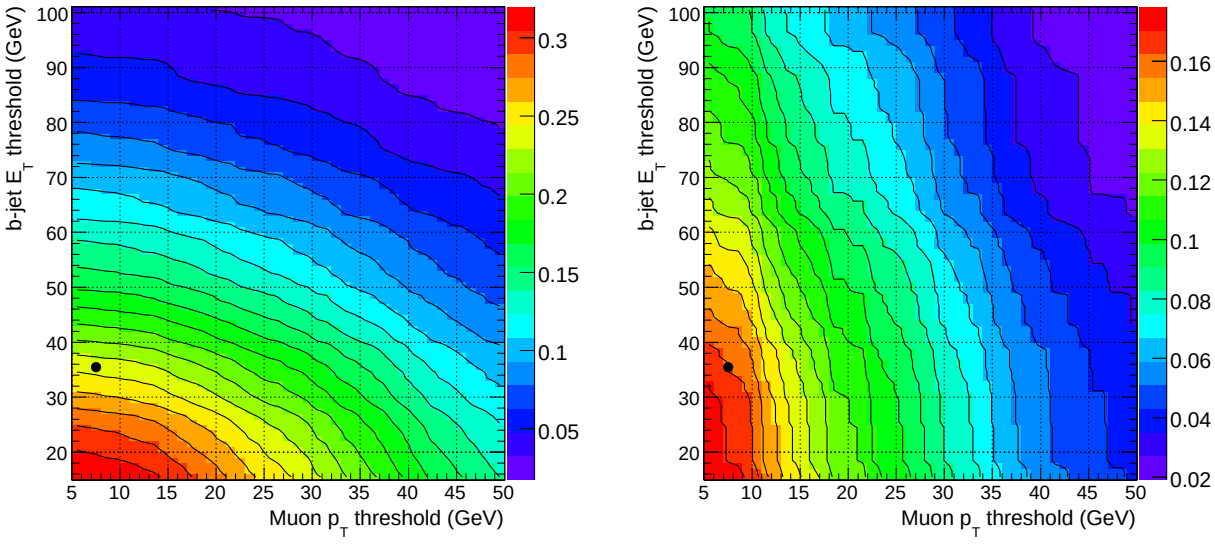

Figure 7.7: HLT efficiency of the muon-plus-b-jet path for $t\bar{t} \rightarrow \mu + jet$ events (left) and SUSY LM1 benchmark point (right) as a function of jet and muon thresholds.

momentum above 4 GeV/c are required to be present. Furthermore, the invariant mass of these two muons should be between 2.0 GeV/c^2 and 4.2 GeV/c^2. This wide mass window is necessary, since the resolution on the invariant mass of the J/ψ meson is found to be 480 MeV/c^2.

At Level-3 partial reconstruction of the Level-2 muon candidates is carried out in the tracker. To define the tracking regions, the primary (interaction) vertex is first identified and reconstructed using only hits in the Pixel detector, with the "Divisive Method" described in reference [14].

The tracking regions are chosen around the direction of the Level-2 muons, with an opening angle of $\Delta R = 0.15$. This small opening angle can be chosen because of the good resolution in both η and ϕ of the muon candidates. All track pairs of opposite charge for which the invariant mass is within 150MeV of the world-average J/ψ mass are retained. The resolution on the invariant mass of the J/ψ meson is found to be 57 MeV/c^2. In addition, the p_T of each muon is required to be above 4 GeV/c and in $|\eta| < 2.5$, and the p_T of the J/ψ candidate above 4 GeV/c. To remove the prompt J/ψ background, the two muon candidates are then fitted to a common decay vertex. The χ^2 of the fit is required to be below 10 and the significance of the transverse decay length is required to be above 3. Furthermore, the transverse momentum of the J/ψ candidate is required to be nearly parallel to its flight path in the transverse plane, since the J/ψ mesons produced in the decays of B_s mesons are collimated around the direction of the B_s meson by the relativistic boost. The cosine of the angle between the reconstructed momentum vector and the vector pointing from the production to the decay vertex is thus required to be larger than 0.9.

7.5.2 Zero-bias and minimum-bias triggers

Since the LHC bunch structure is predetermined, and the bunch-crossings which are filled are know a-priori, we can have Level-1 trigger on each such bunch-crossing and thereby pass "zero-bias" events to the HLT. At high luminosity, with several pp crossings, each such event

Table 7.10: Efficiency ϵ (defined with respect to the number of generated events) and rate R for signal events of the displaced J/ψ trigger selection at low luminosity. Quoted errors are statistical.

Data sample	$B_s \to J/\psi\phi$	$B^+ \to J/\psi K+$	nonprompt $J/\psi \to \mu\mu$
Cross section (nb)	0.074	0.55	94.16
Level-3 ϵ	$(15.4 \pm 1.2)\%$	$(13.5 \pm 0.7)\%$	$(6.4 \pm 0.4)\%$
Level-3 R (Hz)	0.0011 ± 0.001	(0.0074 ± 0.0004)	0.60 ± 0.04

will contain collisions. At lower luminosities a check can be made at the HLT.

There are two implementations for minimum bias triggers. The first one is based on the total energy deposited in the calorimeter, as measured by the Level-1 trigger. The second one is based on charged particle reconstruction with the Pixel detector.

The Pixel-Minimum-Bias HLT algorithm checks that there are N well separated tracks consistent with a single vertex in the expected luminous area. The value $N \geq 2$ maximizes the efficiency of the trigger while keeping the number of wrong decisions at negligible level. The efficiency is 83.7%, consitent with missing diffractive events that are unlikely to give tracks in the pixel acceptance.

The HLT accept rate for the zero- and minimum-bias HLT paths is controlled by the prescales applied at Level-1. We allocate a few Hz to these triggers for the purpose of commissioning and debugging of the rest of the Trigger Menu.

Chapter 8

Trigger Performance for $\mathcal{L} = 10^{32}$ cm^{-2} s^{-1}

The average time taken to form a decision on whether to accept or reject events at the HLT depends significantly on the type of events accepted by the Level-1 trigger. Therefore, a realistic trigger menu is a fundamental ingredient for understanding the CPU time requirements of the HLT selection. The trigger thresholds are typically set by the Level-1 trigger, and the HLT algorithms refine the object identification to significantly improve the purity of triggered objects.

During early LHC operation the trigger system will have to adapt to a wide range of instantaneous luminosities. It is, however, very difficult to simulate a varying luminosity scenario. Instead, the Level-1 trigger menu presented here was optimized for an instantaneous luminosity of $\mathcal{L} = 10^{32}$ cm^{-2} s^{-1} corresponding to the expected run conditions for a significant fraction of the first year of data-taking.

The thresholds for operations at this luminosity were determined by measuring background rates using minimum bias QCD events. The full Level-1 rates are given as a function of thresholds in the Appendix of Ref. [5]. The physics trigger menu is shown in Table 8.1 which lists the names, thresholds, prescale values and rate for each trigger.

8.1 Level-1 Trigger Menu

The Level-1 Global Trigger (GT) logic can accommodate 128 physics trigger bits and 64 technical trigger bits [15]. Not all bits may be active in a given run, whereas some bits may be prescaled. The GT decision is the logical OR of all the active trigger bits. The study presented in this document has not included any technical triggers.

There are six Level-1 object types: μ, isolated e/γ, non-isolated e/γ, central jet, forward jet, τ jet. The GT is given up to four objects of each type. In addition, the GT also uses two event-level quantities, the missing transverse energy and the total transverse energy. The key for the trigger names listed in Table 8.1 is as follows:

- Mu = μ
- IsoEG = isolated e/γ
- EG = isolated e/γ or non-isolated e/γ
- Jet = central jet or forward jet or τ jet
- TauJet = τ jet
- HTT = total hadronic energy
- ETM = missing transverse energy

The trigger conditions require that the E_T (or p_T for μ) of the object in question is equal to or exceeds the threshold indicated. For the studies in this document, single-object triggers with various thresholds are provided to facilitate efficiency measurements for multi-object triggers with the same thresholds.

All the Level-1 triggers presented here are matched to a corresponding HLT path. This is to ensure that the full Level-1 accept rate is utilized by the HLT selection. Doing otherwise would result in an underestimation of the HLT CPU time requirement per Level-1 accepted event.

8.2 Level-1 Trigger Rates

The Level-1 thresholds are set such that there is approximate equity amongst muon, electron, tau, jets and MET triggers. This starting point for allocation of bandwidth will continually be reevaluated after data taking starts. With this initial allocation the lepton thresholds are low enough to capture important W and Z signals to re-establish the Standard Model with CMS. The jet and MET thresholds have a significant overlap with lower energy Tevatron measurements so that QCD extrapolations of jet spectra can be verified. When necessary, e.g., for decays of W and Z to tau leptons, combination triggers are used to lower the thresholds.

The Level-1 trigger rate determined from minimum-bias events is shown in Table 8.1, where the error quoted on the rate is purely statistical. We limited the total Level-1 rate to 16.7 kHz whereas the expected bandwidth available for 2008 (with four DAQ slices) is 50 kHz. This factor three is the standard CMS "safety factor" conceived to account for the large uncertainty in the Level-1 trigger rate estimates arising from uncertainties in the cross sections at the LHC energies, as well as the need to consider a potentially reduced DAQ bandwidth, especially near the startup.

The Level-1 rates have also been computed using a cross-section-weighted mixture of simulated QCD data in several $\hat{p_{\mathrm{T}}}$ bins and dedicated $pp \to \mu X$ sample for $\hat{p_{\mathrm{T}}} > 20$ GeV and $p_{\mathrm{T}}^{\mu} > 3$ GeV. The rates obtained with this mixed sample agree, within statistical errors, with the minbias data shown in Table 8.1.

L1 Trigger	Threshold (GeV)	Prescale	Rate (kHz)
A_SingleMu3	3	1000	0.01 ± 0.00
A_SingleMu5	5	1000	0.00 ± 0.00
A_SingleMu7	7	1	1.11 ± 0.04
A_SingleMu10	10	1	0.47 ± 0.03
A_SingleMu14	14	1	0.18 ± 0.02
A_SingleMu20	20	1	0.09 ± 0.01
A_SingleMu25	25	1	0.06 ± 0.01
A_SingleIsoEG5	5	10000	0.00 ± 0.00
A_SingleIsoEG8	8	1000	0.01 ± 0.00
A_SingleIsoEG10	10	100	0.04 ± 0.01
A_SingleIsoEG12	12	1	2.47 ± 0.06
A_SingleIsoEG15	15	1	1.10 ± 0.04
Continued on next page ...			

L1 Trigger	Threshold (GeV)	Prescale	Rate (kHz)
A_SingleIsoEG20	20	1	0.32 ± 0.02
A_SingleIsoEG25	25	1	0.14 ± 0.01
A_SingleEG5	5	10000	0.00 ± 0.00
A_SingleEG8	8	1000	0.01 ± 0.00
A_SingleEG10	10	100	0.04 ± 0.01
A_SingleEG12	12	100	0.03 ± 0.01
A_SingleEG15	15	1	1.51 ± 0.05
A_SingleEG20	20	1	0.52 ± 0.03
A_SingleEG25	25	1	0.25 ± 0.02
A_SingleJet30	30	1000	0.00 ± 0.00
A_SingleJet70	70	100	0.02 ± 0.01
A_SingleJet100	100	10	0.04 ± 0.02
A_SingleJet150	150	1	0.07 ± 0.01
A_SingleJet200	200	1	0.02 ± 0.01
A_SingleTauJet40	40	1000	0.02 ± 0.01
A_SingleTauJet80	80	1	0.68 ± 0.03
A_SingleTauJet100	100	1	0.20 ± 0.02
A_HTT250	250	1	2.56 ± 0.06
A_HTT300	300	1	0.65 ± 0.03
A_HTT400	400	1	0.08 ± 0.01
A_HTT500	500	1	0.02 ± 0.00
A_ETM20	20	10000	0.00 ± 0.00
A_ETM30	30	1	5.69 ± 0.09
A_ETM40	40	1	0.40 ± 0.02
A_ETM50	50	1	0.05 ± 0.01
A_ETM60	60	1	0.01 ± 0.00
A_DoubleMu3	3	1	0.28 ± 0.02
A_DoubleIsoEG8	8	1	0.28 ± 0.02
A_DoubleIsoEG10	10	1	0.08 ± 0.01
A_DoubleEG5	5	10000	0.00 ± 0.00
A_DoubleEG10	10	1	0.19 ± 0.02
A_DoubleEG15	15	1	0.05 ± 0.01
A_DoubleJet70	70	1	0.58 ± 0.03
A_DoubleJet100	100	1	0.11 ± 0.01
A_DoubleTauJet20	20	1000	0.02 ± 0.01
A_DoubleTauJet30	30	100	0.08 ± 0.01
A_DoubleTauJet40	40	1	2.36 ± 0.06
A_Mu3_IsoEG5	3,5	1	0.95 ± 0.04
A_Mu5_IsoEG10	5,10	1	0.04 ± 0.01
A_Mu3_EG12	3,12	1	0.09 ± 0.01
A_Mu3_Jet15	3,15	20	0.30 ± 0.02
A_Mu5_Jet15	5,15	1	1.62 ± 0.05
A_Mu3_Jet70	3,70	1	0.10 ± 0.01

Continued on next page ...

L1 Trigger	Threshold (GeV)	Prescale	Rate (kHz)
A_Mu5_Jet20	5,20	1	1.18 ± 0.04
A_Mu5_TauJet20	5,20	1	0.66 ± 0.03
A_Mu5_TauJet30	5,30	1	0.38 ± 0.02
A_IsoEG10_Jet15	10,15	20	0.15 ± 0.01
A_IsoEG10_Jet30	10,30	1	1.95 ± 0.05
A_IsoEG10_Jet20	10,20	1	3.04 ± 0.06
A_IsoEG10_Jet70	10,70	1	0.26 ± 0.02
A_IsoEG10_TauJet20	10,20	1	1.95 ± 0.05
A_IsoEG10_TauJet30	10,30	1	1.33 ± 0.04
A_TauJet30_ETM30	30,30	1	1.96 ± 0.05
A_TauJet30_ETM40	30,40	1	0.26 ± 0.02
A_TripleMu3	3	1	0.01 ± 0.00
A_TripleJet50	50	1	0.22 ± 0.02
A_QuadJet30	30	1	0.58 ± 0.03
A_MinBias_HTT10	10	large	0.40
A_ZeroBias	0	large	0.40
Total L1 Trigger Rate (kHz)			16.67 ± 0.15

Table 8.1: Trigger table showing L1 rates at chosen thresholds for $\mathcal{L} = 10^{32}$ cm^{-2} s^{-1}.

8.3 High-Level Trigger Rates

The trigger rates at HLT are determined from a mixture of simulated $\hat{p_{\mathrm{T}}}$-binned QCD as well as dedicated $pp \to \mu X$ samples. This mixed data set is necessary to measure backgrounds for more selective HLT algorithms. In addition, we have added EWK signal rates obtained from $pp \to \gamma\, X$, $W \to e\, \nu_e$, $W \to \mu\, \nu_\mu$, $Z \to e^+e^-$ and $Z \to \mu^+\mu^-$ samples. Table 8.2 summarizes the MC samples used for these trigger studies, and their contributions to the HLT rates.

The trigger rates for all the HLT paths are summarized in Table 8.3, with a total HLT accept rate of approximately 150 Hz. This is a factor of two smaller than the capabilities of the Filter Farm data throughput, estimated to be 300 Hz for an average event size of 1.5 MB. This factor of two is, again, a safety factor that accounts for the overall uncertainty in the current estimates of the HLT accept rate.

While the statistical uncertainties in the HLT rate calculations are improved by using the mixed samples, there are significant systematic uncertainties in some of the trigger rate estimates. As an example, lepton rates from heavy-quark decays are especially difficult to quantify. For this reason, the μ production was enriched by generating dedicated samples which had muons selected at the generator level. These samples are then mixed with the QCD data which provide muons mainly from pion and kaon decays in flight. Double-counting of contributions to muon triggers by the two samples is avoided by explicitly vetoing QCD events with muons in the overlapping region with the muon enriched sample.

Sample description	Cuts	Cross section (pb)	# of events	HLT rate (Hz)
Minimum bias	—	7.92×10^{10}	25 000 000	—-
QCD	$\hat{p_{\mathrm{T}}} \in [0, 15]$ GeV/c	5.29×10^{10}	50 000	0.0 ± 0.0
QCD	$\hat{p_{\mathrm{T}}} \in [15, 20]$ GeV/c	1.46×10^{9}	200 000	11.4 ± 2.7
QCD	$\hat{p_{\mathrm{T}}} \in [20, 30]$ GeV/c	6.32×10^{8}	200 000	23.2 ± 3.1
QCD	$\hat{p_{\mathrm{T}}} \in [30, 50]$ GeV/c	1.63×10^{8}	200 000	28.5 ± 1.5
QCD	$\hat{p_{\mathrm{T}}} \in [50, 80]$ GeV/c	2.16×10^{7}	2 000 000	13.3 ± 0.2
QCD	$\hat{p_{\mathrm{T}}} \in [80, 120]$ GeV/c	3.08×10^{6}	700 000	10.5 ± 0.1
QCD	$\hat{p_{\mathrm{T}}} \in [120, 170]$ GeV/c	4.94×10^{5}	400 000	10.6 ± 0.0
QCD	$\hat{p_{\mathrm{T}}} \in [170, 230]$ GeV/c	1.01×10^{5}	400 000	7.4 ± 0.0
QCD	$\hat{p_{\mathrm{T}}} \in [230, 300]$ GeV/c	2.45×10^{4}	400 000	2.3 ± 0.0
QCD	$\hat{p_{\mathrm{T}}} \in [300, 380]$ GeV/c	6.24×10^{3}	400 000	0.6 ± 0.0
QCD	$\hat{p_{\mathrm{T}}} \in [380, 470]$ GeV/c	1.78×10^{3}	200 000	0.2 ± 0.0
QCD	$\hat{p_{\mathrm{T}}} \in [470, 600]$ GeV/c	6.83×10^{2}	200 000	0.1 ± 0.0
QCD	$\hat{p_{\mathrm{T}}} \in [600, 800]$ GeV/c	2.04×10^{2}	200 000	0.0 ± 0.0
QCD	$\hat{p_{\mathrm{T}}} \in [800, 1000]$ GeV/c	3.51×10^{1}	200 000	0.0 ± 0.0
$W \longrightarrow e\nu$	1 electron with $\lvert\eta\rvert < 2.7$, $p_{\mathrm{T}} > 7$ GeV/c	7.9×10^{3}	1 000 000	0.5 ± 0.0
$Z \longrightarrow ee$	2 electrons with $\lvert\eta\rvert < 2.7$, $p_{\mathrm{T}} > 5$ GeV/c	8.2×10^{2}	1 000 000	0.1 ± 0.0
$W \longrightarrow \mu\nu$	1 muon with $\lvert\eta\rvert < 2.5$, $p_{\mathrm{T}} > 7$ GeV/c	9.8×10^{3}	1 000 000	0.7 ± 0.0
$Z \longrightarrow \mu\mu$	2 muons with $\lvert\eta\rvert < 2.5$, $p_{\mathrm{T}} > 10$ GeV/c	7.9×10^{2}	1 000 000	0.1 ± 0.0
$pp \longrightarrow \mu + X$	$\hat{p_{\mathrm{T}}} > 10$ GeV/c $\mu : p_{\mathrm{T}} > 3$ GeV/c	2.4×10^{7}	4 000 000	23.8 ± 0.3
$pp \longrightarrow \mathrm{jet(s)} + \gamma$	$\hat{p_{\mathrm{T}}} \in [0, 15]$ GeV/c	1.70×10^{8}	100 000	0.0 ± 0.0
$pp \longrightarrow \mathrm{jet(s)} + \gamma$	$\hat{p_{\mathrm{T}}} \in [15, 20]$ GeV/c	2.57×10^{5}	12 000	0.2 ± 0.0
$pp \longrightarrow \mathrm{jet(s)} + \gamma$	$\hat{p_{\mathrm{T}}} \in [20, 30]$ GeV/c	1.32×10^{5}	72 000	0.7 ± 0.0
$pp \longrightarrow \mathrm{jet(s)} + \gamma$	$\hat{p_{\mathrm{T}}} \in [30, 50]$ GeV/c	4.11×10^{4}	22 000	1.4 ± 0.0
$pp \longrightarrow \mathrm{jet(s)} + \gamma$	$\hat{p_{\mathrm{T}}} \in [50, 80]$ GeV/c	7.21×10^{3}	10 000	0.4 ± 0.0

Table 8.2: Summary of MC samples used for the trigger studies of this note. The contribution to the HLT rate does not include prescaled triggers.

While the limited statistics of the lower semileptonic μ b-decays in the generic QCD sample can in principle be corrected for, the QCD mixture was not enriched with electrons coming from b-jets. The limited statistics of the $\hat{p_{\mathrm{T}}}$-binned QCD samples therefore leads to an underestimation of the electron trigger rates. The effect affects mostly the double-electron triggers which have the lower thresholds. Overall, the systematic underestimation of the electron rate (a few Hz) is a small effect compared to the uncertainty on the absolute cross section for heavy-flavor production and can be comfortably accommodated within the safety factors foreseen at both Level-1 and HLT.

HLT path	L1 condition	Thresholds (GeV)	HLT Rate (Hz)	Total Rate (Hz)
Single Isolated μ	A_SingleMu7	11	18.3 ± 2.2	18.3
Single Relaxed μ	A_SingleMu7	16	22.7 ± 1.5	37.7
Double Relaxed μ	A_DoubleMu3	(3, 3)	12.3 ± 1.6	48.5
$J/\psi \to \mu\mu$	A_DoubleMu3	(3, 3) $M_{\mu\mu} \in [2.9, 3.3]$	2.0 ± 0.8	49.4
$\Upsilon \to \mu\mu$	A_DoubleMu3	(3, 3) $M_{\mu\mu} \in [8, 12]$	1.8 ± 0.5	50.5
$Z \to \mu\mu$	A_DoubleMu3	(7, 7) $M_{\mu\mu} \in [80, 100]$	0.1 ± 0.0	50.5
Triple Relaxed μ	A_TripleMu3	(3, 3, 3)	0.1 ± 0.0	50.5
Same-sign double μ	A_DoubleMu3	(3, 3)	5.7 ± 1.2	52.5
$b \to \mu$ tag 1-jet Prescale 20	A_Mu5_Jet15	20 $\Delta R(\mu, j) < 0.4$	4.0 ± 0.1	56.1
$b \to \mu$ tag 2-jets	A_Mu5_Jet15	120, $p_T^{\mathrm{rel}}(\mu) > 0.7$ $\Delta R(\mu, j) < 0.4$	0.5 ± 0.0	56.1
$b \to \mu$ tag 3-jets	A_Mu5_Jet15	70, $p_T^{\mathrm{rel}}(\mu) > 0.7$ $\Delta R(\mu, j) < 0.4$	0.3 ± 0.0	56.1
$b \to \mu$ tag 4-jets	A_Mu5_Jet15	40, $p_T^{\mathrm{rel}}(\mu) > 0.7$ $\Delta R(\mu, j) < 0.4$	0.4 ± 0.0	56.1
$b \to \mu$ tag H_T	A_HTT250	370, $p_T^{\mathrm{rel}}(\mu) > 0.7$ $\Delta R(\mu, j) < 0.4$	2.6 ± 0.2	56.6
$b \to J/\psi(\mu\mu)$	A_DoubleMu3	(4, 4) $M_{\mu\mu} \in [2.95, 3.25]$	0.7 ± 0.1	56.8
μ + b-jet	A_Mu5_Jet15	(7, 35)	0.1 ± 0.0	56.8
$\mu + b \to \mu$-jet	A_Mu5_Jet15	(7, 20)	0.1 ± 0.1	56.8
μ + jet	A_Mu5_Jet15	(7, 40)	6.3 ± 0.7	60.8
$e + \mu$	$\star$	(8, 7)	0.5 ± 0.4	61.2
$e + \mu$ relaxed	$\star$	(10, 10)	0.1 ± 0.0	61.3
$\mu + \tau$	A_Mu5_TauJet20	(15, 20)	0.0 ± 0.0	61.3
Single-Jet	A_SingleJet150	200	9.3 ± 0.1	70.1
Double-Jet	A_SingleJet150 A_DoubleJet70	150	10.6 ± 0.0	74.4
Triple-Jet	†	85	7.5 ± 0.1	78.8
Quad-Jet	‡	60	3.9 ± 0.1	80.5
$\not\!\!E_T$	A_ETM40	65	4.9 ± 0.7	84.0
Acopl. Double-Jet	A_SingleJet150 A_DoubleJet70	125	1.4 ± 0.0	84.0
Acopl. Single-Jet + $\not\!\!E_T$	A_ETM30	(100, 60)	1.6 ± 0.0	84.2
Single-Jet + $\not\!\!E_T$	A_ETM30	(180, 60)	2.2 ± 0.1	84.4
Double-Jet + $\not\!\!E_T$	A_ETM30	(125, 60)	1.0 ± 0.0	84.4

Continued on next page ...

HLT path	L1 condition	Thresholds (GeV)	HLT Rate (Hz)	Total Rate (Hz)
Triple-Jet + $\not\!\!E_T$	A_ETM30	(60, 60)	0.6 ± 0.0	84.4
Quad-Jet + $\not\!\!E_T$	A_ETM30	(35, 60)	1.2 ± 0.1	84.6
H_T + $\not\!\!E_T$	A_HTT300	(350, 65)	4.4 ± 0.1	86.2
Single Jet Prescale 10	A_SingleJet100	150	3.5 ± 0.0	87.9
Single Jet Prescale 100	A_SingleJet70	110	1.5 ± 0.0	89.1
Single Jet Prescale 10^4	A_SingleJet30	60	0.8 ± 0.4	89.9
VBF Double-Jet + $\not\!\!E_T$	A_ETM30	(40, 60)	0.2 ± 0.0	89.0
SUSY 2-jet+$\not\!\!E_T$	A_ETM30	(80,20,60)	2.0 ± 0.1	90.4
Acopl. Double-Jet + $\not\!\!E_T$	A_ETM30	(60, 60)	1.0 ± 0.0	90.4
Single Isolated e	A_SingleIsoEG12	15	17.1 ± 2.3	107.5
Single Relaxed e	A_SingleEG15	17	9.6 ± 1.3	109.3
Double Isolated e	A_DoubleIsoEG8	10	0.2 ± 0.1	109.4
Double Relaxed e	A_DoubleEG10	12	0.8 ± 0.1	109.9
Single Isolated γ	A_SingleIsoEG12	30	8.4 ± 0.7	118.1
Single Relaxed γ	A_SingleEG15	40	2.8 ± 0.2	118.5
Double Isolated γ	A_DoubleIsoEG8	(20,20)	0.6 ± 0.4	119.0
Double Relaxed γ	A_DoubleEG10	(20,20)	1.8 ± 0.5	120.1
High E_T e	A_SingleEG15	80	0.5 ± 0.0	120.4
High E_T e	A_SingleEG15	200	0.1 ± 0.0	120.4
Lifetime b-tag 1-jet	$\diamond$	180	1.3 ± 0.0	120.5
Lifetime b-tag 2-jets	$\diamond$	120	2.1 ± 0.0	121.2
Lifetime b-tag 3-jets	$\diamond$	70	1.7 ± 0.0	121.8
Lifetime b-tag 4-jets	$\diamond$	40	1.8 ± 0.0	122.6
Lifetime b-tag H_T	$\diamond$	470	2.5 ± 0.1	123.1
Single τ	A_SingleTauJet80	(15, 65)	0.2 ± 0.0	123.2
τ + $\not\!\!E_T$	A_TauJet30_ETM30	(15, 35)	1.8 ± 0.2	124.7
Double τ (Calo+Pixel)	A_DoubleTauJet40	15	4.9 ± 0.6	129.4
e + b-jet	A_IsoEG10_Jet20	(10, 35)	0.1 ± 0.0	129.4
e + jet	A_IsoEG10_Jet30	(12, 40)	11.6 ± 1.2	135.8
e + τ	A_IsoEG10_TauJet20	(12, 20)	0.2 ± 0.0	135.8
Prescaled e/γ	See Table 3.9		5.0 ± 0.0	140.8
Prescaled μ	See Table 2.3		3.0 ± 0.0	143.8
Min.Bias	A_MinBias_HTT10	—	1.5 ± 0.0	145.3
Pixel Min.Bias	A_ZeroBias	—	1.5 ± 0.0	146.8
Zero Bias	A_ZeroBias	—	1.0 ± 0.0	147.8
Total HLT rate (Hz)				148 ± 4.9

($\star$): A_Mu3_IsoEG5, A_Mu5_IsoEG10, A_Mu3_EG12
($\dagger$): A_SingleJet150, A_DoubleJet70, A_TripleJet50
($\ddagger$): A_SingleJet150, A_DoubleJet70, A_TripleJet50, A_QuadJet30
($\diamond$): A_SingleJet150, A_DoubleJet100, A_TripleJet50, A_QuadJet30, A_HTT300

Table 8.3: The High-Level Trigger table at $\mathcal{L} = 10^{32}$ cm^{-2} s^{-1}, for an output of approximately 150 Hz.

8.4 HLT Timing Performance

The performance of the full High-Level Trigger Menu is determined by measuring the total HLT processing time when running on various input samples of events accepted by the Level-1 trigger. The times needed to run all HLT paths that had the corresponding Level-1

condition satisfied, including data-unpacking times, are recorded. The relative weights are calculated by taking into account the corresponding cross-section and the combined detector acceptance and efficiency of the Level-1 algorithms.

We find that the major contributions to the average processing time can be attributed to (QCD) minimum bias events in the $0 < p_T < 80$ GeV/c region. The weighted sum of the contributions from all QCD samples and the dedicated mixed samples compares well with the average processing time for Level-1-accepted unbinned minimum bias events. Table 8.4 summarizes the time performance of the High-Level Trigger Menu at $\mathcal{L} = 10^{32}$ cm^{-2} s^{-1} for a Core 2 5160 Xeon processor running at 3.0 GHz. The quoted uncertainty on the combined average processing time is purely statistical and comes from the uncertainties in the determination of the Level-1 emulator efficiencies.

Sample	L1 efficiency (%)	L1 eff. $\times$ σ (pb)	Average time (ms)
Minimum bias	0.19 ± 0.01	$(1.50 \pm 0.09) \times 10^8$	42.7
QCD $\hat{p_{\mathrm{T}}} \in [0, 15]$ GeV/c	0.08 ± 0.01	$(4.36 \pm 0.49) \times 10^7$	31
QCD $\hat{p_{\mathrm{T}}} \in [15, 20]$ GeV/c	2.08 ± 0.11	$(3.04 \pm 0.17) \times 10^7$	36
QCD $\hat{p_{\mathrm{T}}} \in [20, 30]$ GeV/c	5.75 ± 0.18	$(3.64 \pm 0.11) \times 10^7$	40
QCD $\hat{p_{\mathrm{T}}} \in [30, 50]$ GeV/c	21.70 ± 0.41	$(3.54 \pm 0.07) \times 10^7$	47
QCD $\hat{p_{\mathrm{T}}} \in [50, 80]$ GeV/c	63.36 ± 0.84	$(1.37 \pm 0.02) \times 10^7$	53
QCD $\hat{p_{\mathrm{T}}} \in [80, 120]$ GeV/c	95.96 ± 1.23	$(2.96 \pm 0.04) \times 10^6$	73
QCD $\hat{p_{\mathrm{T}}} \in [120, 170]$ GeV/c	99.87 ± 1.18	$(4.93 \pm 0.06) \times 10^5$	143
QCD $\hat{p_{\mathrm{T}}} \in [170, 230]$ GeV/c	100.00 ± 0.00	$(1.01 \pm 0.00) \times 10^5$	264
QCD $\hat{p_{\mathrm{T}}} \in [230, 300]$ GeV/c	100.00 ± 0.00	$(2.45 \pm 0.00) \times 10^4$	385
$pp \to \mu X$	42.96 ± 0.37	$(1.03 \pm 0.01) \times 10^7$	74
$W \to e\nu$	93.18 ± 0.59	$(7.36 \pm 0.05) \times 10^3$	280
$W \to \mu\nu$	84.67 ± 0.80	$(8.29 \pm 0.08) \times 10^3$	123
$Z \to ee$	99.54 ± 0.67	$(8.16 \pm 0.05) \times 10^2$	739
$Z \to \mu\mu$	98.99 ± 1.20	$(7.82 \pm 0.09) \times 10^2$	184
Weighted sum of QCD, W, Z and $pp \to \mu X$ contributions			42.9 ± 5.6

Table 8.4: Average processing wall-clock times for running the High-Level Trigger Menu at $\mathcal{L} = 10^{32}$ cm^{-2} s^{-1} on Level-1-accepted events at an idle Core 2 5160 Xeon 3.0 GHz machine.

Figs. 8.1 and 8.2 show the distributions of the average processing times, including both unpacking and algorithmic portions, for the High-Level Trigger Menu for the weighted sum of QCD contributions in $\hat{p_{\mathrm{T}}} \in [0, 300]$ GeV/c and electro-weak contributions from W & Z production, and unbinned minimum bias events. The two distributions give consistent results, with mean values of 42.9 and 42.7 ms.

8.5 Alternative trigger menus

As can be seen in Table 8.4, the CPU time needed for the HLT selection increases quite rapidly with the $\hat{p_T}$ of the hard scatter. This is some cause for concern, especially for higher instantaneous luminosities, where the trigger thresholds are higher – and therefore the corresponding contributions from higher-$\hat{p_T}$ scatters will be more significant. We have thus attempted to estimate the additional burden on the performance of the HLT algorithms under various scenarios.

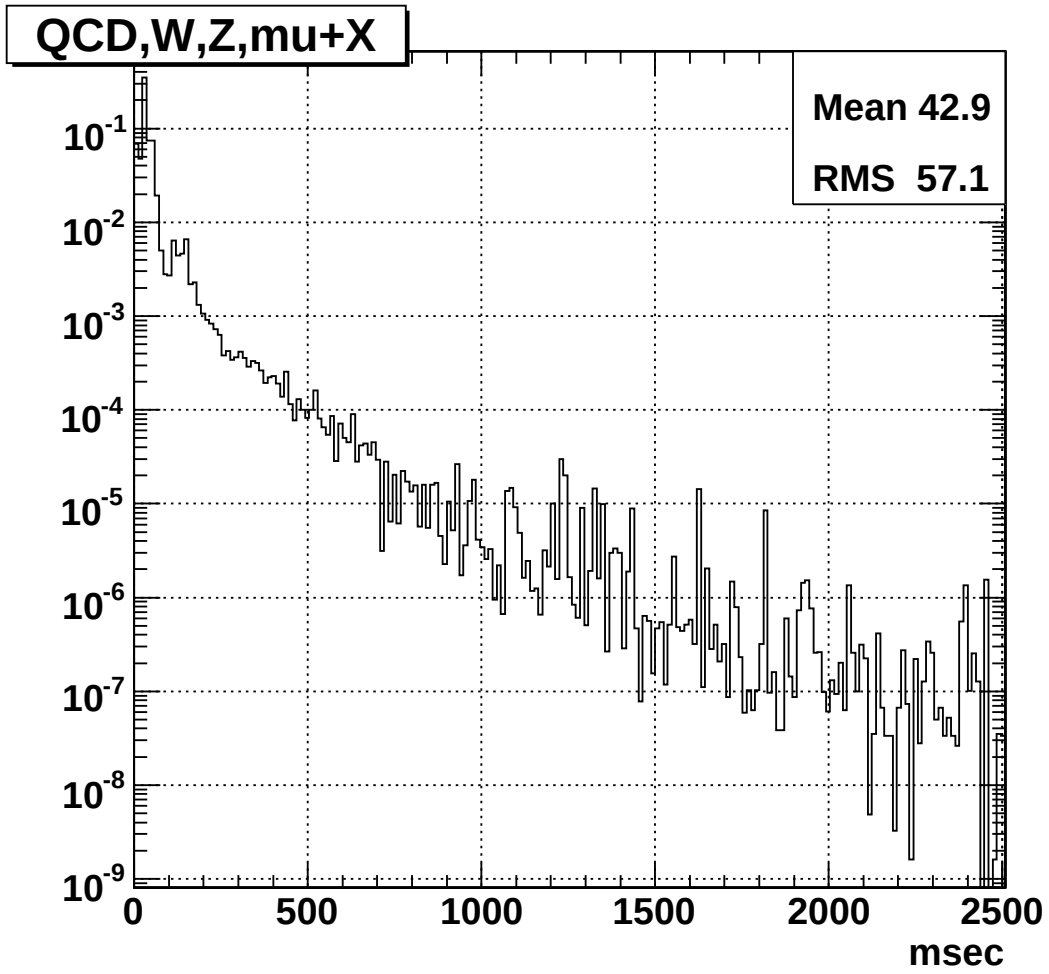

Figure 8.1: Average processing-times (Core 2 5160 Xeon 3.0 GHz) for running the full High-Level Trigger Menu including the data unpacking time. Measurements taken with L1-accepted QCD (0 - 300 GeV/c), EWK (W & Z) and dedicated $pp \rightarrow \mu X$ samples.

In the first scenario we have lowered the thresholds of the single- (80 $\rightarrow$ 60 GeV) and double-tau (40 $\rightarrow$ 35 GeV) Level-1 triggers in an attempt to increase the trigger efficiency for $W/Z \rightarrow \tau$ and Higgs events. To keep the Level-1 accept rate at $\sim$ 17 kHz, we have replaced the L1 condition for various jet and $\not\!\!E_T$ HLT paths from `A_ETM30` to a new `A_HTT100_ETM30` L1 trigger. The modified triggers (L1 and HLT) yield higher efficiencies for $W \rightarrow \tau\nu$ (1.8 % $\rightarrow$ 3.2%) and $H \rightarrow \tau\nu$ (16 % $\rightarrow$ 27% for M_H = 200 GeV/c^2, or 29 % $\rightarrow$ 39% for M_H = 400 GeV/c^2), and $Z \rightarrow \tau\tau$ (8.6% $\rightarrow$ 12%). The average processing time for the new Trigger Menu increases to 45.8 ms (calculated with minimum bias Level-1-accepted events) or 45.2 $\pm$ 3.4 ms (calculated with the weighted sum of QCD and electro-weak samples of Level-1-accepted events).

In the second scenario we have increased the thresholds of all Level-1 triggers according to the $\mathcal{L} = 2 \times 10^{33}$ cm^{-2} s^{-1} Trigger Menu presented in Ref. [3]. The Level-1 efficiencies of the samples listed in Table 8.4 are calculated for the trigger menu presented in Physics TDR Vol. II, and the relative contributions are scaled accordingly. Assuming that the processing time for the HLT algorithms for each of the samples remains the same, we calculate an average

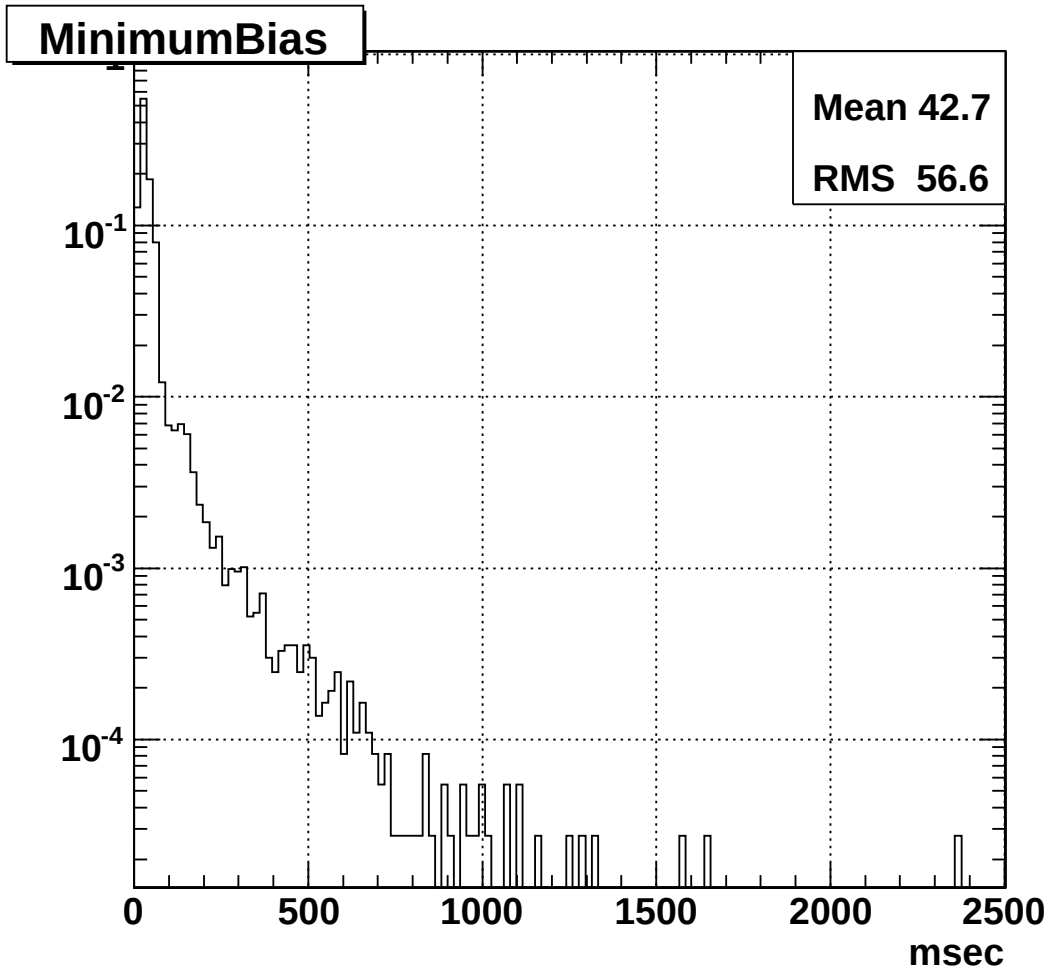

Figure 8.2: Average processing-times (Core 2 5160 Xeon 3.0 GHz) for running the full High-Level Trigger Menu including the data unpacking time. Measurements taken with L1-accepted unbinned minimum bias sample.

time of 55.6 ± 4.2 ms. In a more realistic study where the performance of the HLT algorithms would be evaluated including pile-up, it is expected that the increase on the average HLT processing time would be somewhat higher.

In both cases the variations on the estimate of CPU requirement are not large, thus lending support to the central estimate for the trigger table presented here. Furthermore, the range of values quoted can be thought of, conversely, as an indication that the HLT selection maintains some flexibility margin.

Naturally, the trigger tables which will actually be utilized will be further optimized, in terms of both their physics and CPU performance, in the time remaining before the data-taking in 2008. Most importantly, the HLT will be tuned significantly with the first LHC data.

8.6 Future improvements

A series of additional optimization steps have been planned for the HLT. The focus is the major contributions to the average processing time of the HLT algorithms, as identified by profiling studies using simulated minimum bias events accepted by the Level-1 trigger. Some of the areas of the expected improvements are:

- Implementation of regional data-unpacking in all subdetectors by using the L1 objects as seeds. A major finding of the profiling studies was the vast memory allocation and deallocation by the HLT code. By limiting the data-unpacking in regions specified by the Level-1 reconstruction, we expect significant speed improvements on both the digitization process of the "raw" data and the local reconstruction of the hits for the corresponding subdetector. This will also make HLT unpacking times less susceptible to any detector noise problems which will be masked in the L1 trigger. Regional unpacking was implemented for the ECAL system for muon and electron/photon HLT paths for this study, giving approximately a factor of four improvement over the full ECAL unpacking approach. Similar gains are expected for the rest of the HLT paths and subsystems.
- Further optimizations obtained in various areas of the `CMSSW` code involving unnecessary data-copying and sorting. Examples are the migration of the `CMSSW` tracking code from the `CLHEP` to `ROOT`'s `SMatrix` library (a factor of two improvement has been achieved in newer software releases), or usage of unsorted data-containers when possible.
- Introduction of a "time-out" mechanism that would stop the execution of HLT algorithms and accept the event as soon as the processing time exceeds a limit (e.g. 600 ms). The motivation here is to limit the dependence of the average processing time on events that take significantly long times to process, possibly with complex topologies that are difficult to reproduce in a Monte Carlo simulation. The timed out events will be stored for both normal data processing and validation of future HLT algorithms.

The above list refers to the improvements that are currently either planned or already underway. The first collision data from the LHC should yield extremely useful information in further optimizing the trigger algorithms, the thresholds employed as well as the overall CPU performance of the system.

Chapter 9

Summary

The current note presents the most extensive study of the High-Level Trigger algorithms, software, rates, efficiencies and technical requirements to this date. As stated in the introduction, all the algorithms were developed, tested and run within the latest software framework, CMSSW. The detector geometry simulated reflects the most up-to-date understanding of the detector layout, whereas the reconstruction code, which is still based on the offline reconstruction as much as possible, has advanced considerably since the early versions presented in the Data Acquisition TDR where the HLT was first presented. For the first time, the actual RAW data format expected from the CMS readout has been simulated and the code for unpacking the data was deployed and included in all timing studies. On the Level-1 trigger front the major improvement has been the deployment of the Level-1 trigger emulator which led to a more realistic set of events that are input to the HLT.

The study has concentrated on the startup conditions, and therefore the trigger table developed provides estimates of the thresholds and corresponding trigger rates for an instantaneous luminosity of 10^{32} cm^{-2} s^{-1}. As with all previous studies of rates, the trigger menu has explicitly allocated only one third of the maximum Level-1 trigger bandwidth of 50 kHz, to account for all the conditions that the current physics generators and detector simulation do not simulate as well as potential, the uncertainties in key cross sections (e.g. for jet production) and potential deviations from the maximum readout rate of 50 kHz. Examples of conditions not included in the simulations include the general beam conditions, interactions upstream of the CMS detector, detector effects such as noise spikes and potential problems with the electronics and/or readout of some sub-detectors, especially during the commissioning phase of the experiment. These effects depend on a host of conditions that, as the previous generations of experiments have shown, are indeed very difficult to simulate.

A second "safety factor" has been applied to the accept rate of the HLT: only half of the maximum bandwidth of 300 Hz has been explicitly allocated in the trigger menu. This factor accounts for all the uncertainties in the cross sections of the processes that have been simulated as well as uncertainties in the details of the simulation of the backgrounds simulated with the Monte Carlo generators. As examples, we cite the cross section for jet and heavy-flavor production for which we have used the lowest-order cross sections. On the simulation side a good example of a process with significant uncertainties is the fake rate for electrons per jet. Experience from previous and currently active experiments shows that this rate cannot be estimated with high precision prior to data-taking (and remains difficult to simulate even after the first data are collected).

With these two safety factors the resulting trigger table has used an accept rate of 17kHz at Level-1 and an accept rate of 150 Hz at the HLT. As shown in this document, this yields

high efficiency for the signatures that constitute the major physics goals of CMS. Moreover, a long-standing issue, that of the CPU requirement of the HLT has been addressed. The current estimates, using a processor which is close to the type that will be used at the startup yields a figure of ≈ 40 ms per event. This was the figure estimated in the DAQ TDR back at the end of 2002. It is remarkable that that original figure which utilized significant factors in extrapolating the conditions in 2007 has been achieved one year ahead of data-taking.

Analysis of the CPU time requirements displays a strong dependence on the complexity of the events passing the Level-1 trigger, thus leading to the expectation that the CPU requirements will increase as the instantaneous luminosity will rise with time. As explained in the performance chapter, however, further improvements are expected in the performance of the HLT in the near future. These vary from further optimization of the algorithms employed (e.g. using regional reconstruction and unpacking everywhere) to software code improvements and finally changes to the operational plans of the filter farm (acceptance of complex events). Our current estimates are that the overall CPU needs will remain within the resources available and CMS will thus be able to concentrate on the optimization of the physics selection online.

In summary, the current study is the first end-to-end test of the HLT that includes all elements from the RAW-data to a full estimate of the event overlaps across HLT paths. The results are very encouraging: despite the injection of more realism into the simulations, the physics performance remains intact, whereas the resources required are well within the CMS plans. It remains to subject this system to real data from LHC collisions.

References

Notes:

a) CMS Notes are available at `http://cms.cern.ch/iCMS/` unless otherwise noted.

b) References marked **doi** should be prefixed with `http://dx.doi.org/`.

---

[1] CMS Collaboration, "The TriDAS Project Technical Design Report, Volume 2: Data Acquisition and High-Level Trigger," *CERN/LHCC* **2002-26** (2002). CMS TDR 6.2.

[2] CMS Collaboration, "The CMS Physics Technical Design Report, Volume 1," *CERN/LHCC* **2006-001** (2006). CMS TDR 8.1.

[3] CMS Collaboration, "The CMS Physics Technical Design Report, Volume 2," *CERN/LHCC* **2006-021** (2006). CMS TDR 8.2.

[4] CMS Collaboration, "The TriDAS Project Technical Design Report, Volume 1: The Level-1 Trigger," *CERN/LHCC* **2000-38** (2000). CMS TDR 6.1.

[5] CMS Collaboration, "CMS High Level Trigger," *CMS Note* **2007/009** (2007).

[6] N. Amapane et al., "High Level Trigger Algorithms for Muon Isolation," *CMS Note* **2002/040** (2002).

[7] N. Amapane et al., "Methodology for the Simulation of Single-Muon and Di-Muon Trigger Rates at the CMS Experiment in the Presence of Pile-Up," *CMS Note* **2002/042** (2002).

[8] L. Agostino and M. Pieri, "HLT Selection of Electrons and Photons," *CMS Note* **2006/078** (2006).

[9] R. Harris et al., "Jet Performance in CMSSW_1_2_0," *CMS Note in preparation* (2007).

[10] S. Esen and R. M. Harris, "Jet Triggers and Dijet Mass," *CMS Note* **2006/069** (2006).

[11] S.Gennai et al., "Tau jet reconstruction and tagging in CMS," *EPJ C Direct* **10.1140/epjcd/s2006-02-001-y** (2006).

[12] M.Vos and F.Palla, "B Tagging in the High Level Trigger," *CMS Note* **2006/030** (2006).

[13] I.Tomalin et al., "Supplementary information on b-lifetime tagging in the high level trigger," **CMS Twiki** (2007).

[14] S.Cucciarelli, M.Konecki, D.Kotlinski, and T. Todorov, "Track reconstruction, primary vertex finding and seed generation with the Pixel Detectors," *CMS Note* **2006/026** (2006).

[15] C.-E. Wulz et al., "Concept of the CMS First Level Global Trigger for the CMS Experiment at LHC," *Nucl. Ins. Meth.* **A473/3 (231-242)** (2001).